Title:

The high-throughput perturbation of long non-coding RNA reveals functional features in stem cells and across cell-types

Authors:

Chi Wai Yip[1], Chung-Chau Hon[1], Kayoko Yasuzawa[1], Divya M. Sivaraman[1,2], Jordan A. Ramilowski[1,3], Youtaro Shibayama[1], Saumya Agrawal[1], Anika V. Prabhu[1], Callum Parr[1], Jessica Severin[1], Yan Jun Lan[1], Josée Dostie[4], Hiromi Nishiyori-Sueki[1], Michihira Tagami[1], Masayoshi Itoh[1], Fernando López-Redondo[1], Tsukasa Kouno[1], Jen-Chien Chang[1], Joachim Luginbühl[1], Masaki Kato[1], Mitsuyoshi Murata[1], Wing Hin Yip[1], Xufeng Shu[1], Imad Abugessaisa[1], Akira Hasegawa[1], Harukazu Suzuki[1], Ken Yagi[1], Takeya Kasukawa[1], Michiel de Hoon[1], Piero Carninci[1,5], Jay W. Shin[1,*]

Affiliations:

1. RIKEN Center for Integrative Medical Sciences, Yokohama, Kanagawa 230-0045 Japan
2. Sree Chitra Tirunal Institute for Medical Sciences and Technology, Kerala 695 011 India.
3. Advanced Medical Research Center, Yokohama City University, Yokohama, Kanagawa 236-0004 Japan
4. Department of Biochemistry, Rosalind and Morris Goodman Cancer Research Center, McGill University, Montréal, Québec, Canada
5. Human Technopole, via Rita Levi Montalcini 1, Milan, Italy

* Correspondence: jay.shin@riken.jp

Abstract

Long non-coding RNAs (lncRNAs) were shown to regulate pluripotency and differentiation, however, a comprehensive assessment of their regulatory roles in stem cells is currently lacking. By performing a large-scale knockdown of lncRNAs (n = 390) in human induced pluripotent stem (iPS) cells, we systematically characterized their roles in self-renewal and pluripotency. Cell growth and transcriptomic assays revealed respectively, 18.3% and 29.3% of these lncRNAs in altering cellular and molecular phenotypes upon knockdown. By integrating the molecular phenotypes with chromatin-interaction assays, we identified their *cis*- and *trans*- interacting partners as potential primary targets. In addition, cell-type enrichment revealed 16 lncRNAs associated with pluripotency and we highlighted *LINC02595*, *CATG00000090305.1* and *RP11-148B6.2*. Next, we integrated fibroblasts phenotyping data (Ramilowski et al., 2020; Genome Research) and reported that only 2.9% lncRNAs exhibited consistent cell growth phenotype, while molecular phenotype showed 66.7% agreement. This highlights their consistent primary functional roles across cell-types and the distinct secondary effects under different cellular environments.

Keywords: Long noncoding RNA, iPS, functional annotation, CAGE

Introduction

The effort to characterize the human transcriptome[1,2] has revealed a large collection of long noncoding RNAs (lncRNAs), which are pervasively transcribed with little or no protein coding potential. Most lncRNAs are transcribed by RNA polymerase II and they are frequently capped, spliced and polyadenylated.[3] While an increasing number of lncRNAs have been identified in mediating multiple regulatory processes,[4] experimentally curated functional lncRNAs represent less than 1% of all known lncRNA transcripts.[5,6] While most lncRNAs are expected to acquire function over evolutionary time,[7] a genome wide analysis of 1829 samples of human cell-types or tissues further indicated 69% of lncRNAs with functional insights.[1] To better address cell-type specific functional lncRNAs, a loss-of-function genetic screen of lncRNAs is vital.[8]

Human induced pluripotent stem (iPS) cells are reprogrammed from somatic cells by introducing the exogenous expression of the transcription factors OCT3/4, SOX2, KLF4 and c-Myc.[9] Although minor differences amongst iPS cells[10] and between iPS cells and embryonic stem (ES) cells[11] are observed, iPS cells functionally resemble ES cells by

forming embryoid bodies or teratomas, and undergoing lineage specific differentiations. Recent studies in human ES cells and iPS cells showed indispensable roles of lncRNAs for their self-renewal and differentiation. For example, *lncRNA-ES1, lncRNA-ES3 and FAST* play a role in maintaining pluripotency,[12,13] *LINC-ROR* in cell reprogramming[14] and self-renewal,[15] and *TUNA* in neuronal differentiation.[16] Furthermore, pervasively expressed lncRNAs are associated with more active and open chromatin observed in pluripotent cells.[3] LncRNAs with higher diversity and expression level provided pluripotent cells an attractive model in lncRNA functional annotation. Indeed, genetic screens of lncRNAs revealed iPS cells with the highest percentage of functional lncRNAs among several cell-types.[17]

Genetic screens using DNA-targeting technologies such as CRISPRi[17] and CRISPRa[18] or RNA-targeting technologies such as RNAi[19] and LNA gapmer[8] have demonstrated systematic strategies to annotate novel lncRNA function. Many screening designs rely on the cellular phenotypic outcome, leading to the discovery of cell survival-related functions, while lncRNAs with other functional roles were less explored. In addition, due to the tissue-specific expression pattern of lncRNAs,[20] the functions of specific sets of lncRNAs are only revealed under specific cell-types and conditions. Studying the same lncRNAs across cell-types and conditions will bring further insights into lncRNA biology.

We have previously characterized 285 lncRNAs in human dermal fibroblast (HDF) primary cells by targeting the RNA molecules.[8] In this screening platform, we adopted LNA gapmer antisense oligonucleotides (ASOs) to directly target RNA molecules, and streamlined this with cellular phenotyping and transcriptomic profiling to reveal functional roles. While the cell growth phenotype revealed lncRNA function in self-renewability of iPS cells, molecular phenotyping explored their roles in molecular pathways related to pluripotency and others. By perturbing 390 lncRNAs in the human iPS cells, we identified functional lncRNAs at both the cellular and molecular phenotypic levels (**Fig. 1**). RNA-DNA and DNA-DNA interaction data were integrated to the knockdown profiles to identify primary gene targets. Three novel lncRNAs regulating pluripotency were identified and validated. To comprehensively compare the properties and functions of lncRNAs across different cell-types, we selected the lncRNAs robustly expressed in both HDF and iPS cells, and performed knockdown by the same set of ASOs. We observed cell-type specificity in the growth phenotype but broader consistency in molecular phenotype, implying distinct growth phenotypes may be due to different secondary responses between the cell-types.

Results

Properties of 390 lncRNA targets

We selected 390 lncRNAs expressed in iPS cells and designed 5 to 10 ASOs per lncRNA to specifically suppress their expression in iPS cells. These lncRNAs cover a broad range of expression levels in iPS cells (**Fig. S1a**) and a broad range of cell-type specificity amongst 71 cell-types (**Fig. S1b**), with 102 lncRNAs overlapping with the targets tested in our previous study in HDF.[8] These lncRNAs are generally categorized as either antisense, divergent, intergenic or sense intronic, and 12.3% of the lncRNAs are derived from enhancer-like regions **(Fig. S1c**). Subcellular fractionation analysis revealed 33% of the lncRNAs are enriched in the chromatin, 23% in the nucleoplasm and 44% in the cytoplasm (**Fig. S1d-e**). Notably, they were selected to represent lncRNAs commonly expressed in stem cells and their expression levels in the iPS line of this study highly correlate with that in other iPS and ES cell lines (**Fig. S1f**).

Cellular phenotyping unveils lncRNAs influencing self-renewal

After knockdown of each ASO (n = 2225), we measured its knockdown efficiency using RT-qPCR, and its effect on cell growth (i.e. cellular phenotype) using a real-time imaging-based growth assay, comparing against non-targeting negative control (NC) ASO as background. We found 756 out of 2225 ASOs with knockdown efficiency ≥ 50% (i.e. effective ASOs) and 202 lncRNAs with ≥ 2 effective ASOs (**Fig. 2a, Table S1**). The growth assay revealed 178 out of the 756 effective ASOs to significantly inhibit cell growth (Student's t-test, p-value < 0.05; **Fig. 2b, S2a-b**). This observation was further supported by an independent optical density-based WST-1 growth assay, which strongly correlated with the image-based growth assay (**Fig. 2c**). Notably, ASOs with effective knockdown showed significantly stronger growth inhibition (Wilcoxon test, $p < 0.05$, **Fig. 2d**) and ASOs targeting the same lncRNA showed a significant concordance of the normalized growth rate (Methods; **Fig. 2e**). These results suggest the observed growth inhibition is likely attributed to the specific effects of lncRNA knockdown instead of general effects (e.g. ASO toxicity). Among the 202 lncRNAs with successful knockdown, 37 (~18.3%) had 2 or more growth inhibiting ASOs (robust cutoff) while 12 (~5.9%) were statistically significant based on binomial test at p-value < 0.05 (stringent cutoff; methods; **Fig. 2f**).

We next asked whether different properties of the lncRNAs are correlated with the successful knockdown (≥ 2 effective ASOs) and growth inhibition (≥ 2 growth inhibiting ASOs). We found that lncRNAs with successful knockdown are more enriched in the nucleus, have a higher number of exons, higher expression levels, lower exosome sensitivity, and lower cell-type specificity (**Fig. 2g, S2c**). Additionally, the lncRNAs with growth inhibition exhibited significantly higher expression level and lower cell-type specificity (**Fig. 2g-h, Table S2**).

Molecular phenotypes recapitulate cellular phenotypes

To investigate the effect of lncRNAs knockdown on transcriptome (i.e. molecular phenotype), we performed Cap Analysis of Gene Expression (CAGE) [21,22] after knockdown with selected effective ASOs (n = 317, targeting 123 lncRNAs). For each ASO, we performed differential gene expression, pathway enrichment and differential transcription factor binding motif analyses, comparing against the NC ASO background (Methods). First, to identify lncRNAs whose knockdown led to reproducible and significant transcriptome global change, we paired the ASOs targeting the same lncRNA (same-target-ASO-pair, 293 pairs), and compared the mean distance of each pair against a null distribution of permuted pairs of NC ASO replicate (NC-ASO-pairs). We quantified the distance based on the overall extent of transcriptome changes for each ASO using Kolmogorov's *D* (refer to as distance, Methods). This resulted in 52 significant same-target-ASO-pairs targeting 28 (~22.7%) lncRNAs (empirical *p*-value < 0.01 and Wilcoxon test FDR < 0.05; Methods; **Fig. 3a**). We observed a strong correlation between the overall extent of transcriptome changes and the extent of growth inhibition (**Fig. S3a-b**), suggesting that gene programs such as apoptosis or inhibition of cell growth induces global shift in the transcriptome. Consistently, the pathway enrichment related to cell growth, e.g. cell cycle and cell death, are highly correlated with the normalized growth rate (Methods, **Fig. 3b, S3c**). These analyses revealed a general agreement between two independent measurements: the molecular and cellular phenotypes.

Analysis of molecular phenotype indicates functional features of lncRNAs

Next to identify impacted molecular features for ASO, we first implemented the Jaccard index to test the concordance of differentially expressed genes (methods). We found that the mean Jaccard index of the same-target-ASO-pairs is significantly higher than the null distribution from permuted different-target-ASO-pairs (empirical *p*-value < 0.05; **Fig. S3d**), suggesting that the observed ASO effects are generally target-specific. This observation is

also supported by a more stringent analysis incorporating the Wilcoxon test (empirical FDR < 0.05; **Fig. S3e-f**).

To identify lncRNAs with reproducible molecular phenotypes by 2 or more ASOs, we implemented a reciprocal enrichment method to identify ASO-pairs leading to concordant transcriptomic effects (Methods; **Fig. S4a-c**). This method significantly distinguishes same-target-ASO-pairs against different-target-ASO-pairs (empirical *p*-value < 0.05; **Fig. S4d**). Overall, 36 ASO-pairs (**Fig. 3c, S4e**), which account for 22 lncRNAs, showed concordant transcriptomic effects upon knockdown. Hereby, we identified 43 lncRNAs which showed reproducible transcriptome global changes (n = 28) and/or concordant transcriptomic effects (n = 22) with the support of ≥ 2 ASOs (**Fig. 3d**).

Next, we sought to define optimal cutoffs for identifying significant molecular features (i.e. genes, pathways and transcription factor binding motifs) after ASO knockdown, by maximizing the ratio of concordance of same-target-ASO-pairs to different-target-ASO-pairs (Methods; **Fig. S4f**). At these optimal cutoffs, the median number of significant differentially active genes, pathways and motifs of the 317 ASO knockdowns were respectively, 11, 25 and 0 (**Fig. 3e**). Among the 43 lncRNAs with reproducible knockdown effects, 36 of them showed at least one common differentially active molecular feature. These 36 lncRNAs are defined as showing functionally reproducible molecular phenotypes (**Fig. 3f, Table S3**). We compared these 36 lncRNAs showing molecular phenotypes with the others (n = 87) for genomic property enrichment but no significant enrichment was found (**Table S2**).

Primary gene target at chromatin level

LncRNAs regulate cellular activity by multiple mechanisms,[23] with the majority of the experimentally curated lncRNAs acting via transcriptional regulation.[6] However, the primary gene target of a lncRNA is not distinguishable from the secondary responses in the molecular phenotype. To elucidate the primary effects of lncRNAs from their physical associations with chromatin, we integrated the molecular phenotype with Hi-C and RADICL-seq, a method to capture RNA-DNA interactions,[24] from the native iPS cells.

We identified the protein-coding genes in contact with the lncRNAs from their DNA loci and the RNA molecules, which are reflected by Hi-C and RADICL-seq respectively. From the 123 lncRNAs assayed for transcriptomic response, 121 of the lncRNA loci showed significant Hi-C contacts (FDR < 0.05), resulted in 3066 lncRNA-protein-coding gene pairs. From the RADICL-seq results, 115 lncRNAs showed significant contacts (FDR < 0.05) and

2059 lncRNA-protein-coding gene pairs were identified. Consistent with the previous studies,[25,26] the significant pairs of DNA-DNA and RNA-DNA interactions are largely overlapped (**Fig. S5a**). We thereby considered the 3066 pairs with Hi-C contacts as *cis* interactions (121 lncRNAs) while those pairs with RADICL-seq support alone and with at least 1 Mb apart as *trans* interactions (n = 893, from 64 lncRNAs). Additionally, eQTL-genes[27] with the variants located in the promoters and gene bodies of the lncRNA targets were integrated, showing 102 lncRNAs with detectable eQTL-genes (**Fig. S5b**)

By integrating the significant DEGs and significant contact genes of the lncRNAs, we showed that globally *cis* and *trans* interactions enriched with DEGs (**Fig. S5c**). Then, we directly link the significant DEGs with *cis* interactions of each lncRNA. We identified 28 lncRNAs with primary targets in *cis* (**Fig. 4a**, full list in **Table S4**). One of the significant pairs is the lncRNA *TUG1* and protein-coding gene *SELENOM*, which are located in the same TAD, with significant Hi-C and RADICL-seq contacts (**Fig. 4b**). *TUG1* knockdown reduced the expression of *SELENOM* in CAGE and was independently validated by RT-qPCR (**Fig. 4c**). *TUG1* and *SELENOM* share similar phenotypic outcomes where they mediate cell proliferation in multiple cancers[28–31] and obesity.[32,33] In addition, we revealed that the lncRNA *RNASEH1-AS1*, without affecting the expression of *RNASEH1*, regulated *ADI1* in *cis*, supported by an independent knockdown and RT-qPCR (**Fig. S5d-e**).

Next, we performed an enrichment test on the *cis*-contacted protein-coding genes to the ranked transcriptomic response (Methods) for each lncRNA. The result revealed a significant enrichment of the *cis*-contacts for *CATG00000087927* and *LINC00240* (adjusted p-value < 0.05; **Fig. S5f**), implying these lncRNAs may exhibit strong *cis*-regulatory effects towards multiple genes spatially nearby and regulate cell growth pathways (**Fig. S5g**). Enrichment analysis on the eQTL-genes with the variants located in the lncRNA targets further highlighted *LINC00240*, at which multiple eQTL-genes were regulated upon the knockdown of *LINC00240* (**Fig. S5h**).

We integrated the transcriptomic profiles with *trans* interactions to investigate potential *trans*-acting lncRNAs. We performed pair-base identification combined with complementary sequence similarity detection between lncRNA targets and gene DNA sequence, and discovered 6 novel *trans*-acting lncRNAs (**Fig. 4d,** full list in **Table S4**) including *CATG00000090305* (**Fig. S6a-b**). Besides, Enrichment analysis revealed *CATG00000090305* and *FIRRE* as the top hits, followed by other lncRNAs such as *LINC02595* (p-value < 0.05)

(**Fig. S6c-d**). *FIRRE* has been previously reported as a *cis*- and *trans*-regulating lncRNA that regulates genes within and outside of chromosome X.[34,35] Overall, we showed that the integration of the genome-wide static chromatin interaction data and the loss-of-function transcriptomic responses of 123 lncRNAs, effectively identified the primary target genes of some lncRNAs.

LncRNA modulates cell identities

To elucidate the differentiation potential of lncRNA in stem cells, we tested if lncRNA knockdown correlates with predefined cell-type signatures. We derived the cell-type specificity score from 71 cell-types including iPS and ES cells by applying the Gini index (Methods; **Table S5**). After identifying the top specific genes from each cell-type as genesets (Methods), we performed geneset enrichment analysis against the molecular phenotype data. We additionally included genesets from *POU5F1* knockdown transcriptomic responses to represent pluripotency-related genes. The knockdown profiles from *POU5F1* and 4 other lncRNAs showed significant depletion of stem cell related genesets while 12 lncRNAs showed enrichment in stem cell related genes (**Fig. 5a**). Additionally, we found 24 lncRNA knockdown data with enrichment in various cell-type specific genesets (**Fig. S7a**). For example, knockdown of *NUTM2B-AS1*, which was recently shown to be involved in a neuromuscular disorder,[36] was enriched in the neuron cell-type. Knockdown of *TUG1* reflects negative enrichment of osteoblast, tendon and fat cells, with *TUG1* promoting osteogenic differentiation from periodontal ligament stem cells[37] and tendon stem cells,[38] as well as promoting brown remodeling of white adipose tissue.[33]

To validate the role of lncRNAs which modulate stem-cell identity, we performed a colony formation assay with lncRNA knockdown. The knockdown of the pluripotency-supporting lncRNAs *CATG00000090305.1* and *RP11-148B6.2*, showed a decrease in colony formation. Alternatively, the knockdown of *LINC02595*, which hinders stem cell molecular phenotype, increased the number of colonies (**Fig. 5b**). This shows that these lncRNAs affect the cell survival of iPS cells at the single cell stage.

We further investigated the role of *LINC02595*, as one of the 12 lncRNAs found hindering the stem cell molecular phenotype. Knockdown of *LINC02595* down-regulated *HDAC6* and up-regulated *POU5F1* and *POU5F1B* under spontaneous differentiation conditions (**Fig. 5c**). Notably, *HDAC6* was shown to be regulated by *LINC02595* in *trans* (**Table S4**) and *HDAC6* level increases along differentiation from iPSC to neurons in the Fantom5 analyses.[1] *HDAC6*

translates to histone deacetylase and suppresses multiple genes during differentiation.[39] Inhibition of it up-regulated OCT4 in porcine blastocysts[40] while HDAC inhibitor was shown to improve iPS cell reprogramming from peripheral blood mononuclear cells.[41]

Extent of lncRNA function across cell-types

LncRNAs are known to exhibit cell-type and tissue-specific expression, and cell-type specificity is generally higher than mRNA (**Fig. 6a**).[20] To explore the role of distinct subcellular localization of lncRNAs in different cell-types, we performed fractionation on HDF and iPS cells for subcellular RNA-seq and showed that subcellular enrichment is similar between lncRNA and mRNA across all the expression levels (**Fig. 6b**). Consistent with a previous study, [42] this analysis suggests that many lncRNAs tend to maintain their subcellular localization, which largely dictates the functions of lncRNAs.[43] Thus, we reasoned lncRNAs that express ubiquitously across cell-types exhibit similar molecular roles.

To test this hypothesis, we analyzed lncRNAs from two functional genetic screens: HDF[8] and iPS cells (this study). We found 102 lncRNA targets are common and they have comparable expression levels and subcellular localizations in both cell-types, with a variety of specificity scores (**Fig. S1a-b, S8a**). Among them, 69 lncRNAs showed successful knockdown by at least 2 independent ASOs in both cell-types, and exhibited a positive correlation for the knockdown efficiency between two cell-types (**Fig. 6c, Fig. S8b-c**). However, the cell growth phenotype correlation was low (Jaccard index of 5.7%; **Fig. 6c, Fig. S8d-e**), which agrees with a previous study on distinct growth phenotypes mediated by the same lncRNA loci across cell-types.[17] Additionally, the differential expression level of lncRNAs between HDF and iPS cells was found to contribute to the distinct growth phenotypes (**Fig. S8f**), which echoes our finding that the expression level of lncRNAs correlate with growth phenotypes (**Fig. 2g-h**).

We took advantage of the molecular phenotype data of 33 common lncRNAs and explored the lncRNA functional specificity across the two cell-types. To compare molecular phenotypes from two cell-types, we performed the reciprocal enrichment test for ASOs targeting the same lncRNA (Methods; **Fig. S4a-c**). Notably, the same-target-ASO-pairs across the two cell-types resulted in a higher concordance than the different-target-ASO-pairs (empirical p-value < 0.0001; **Fig. S9a**). Specifically, 59 ASO pairs, or 26 lncRNA targets, showed concordant transcriptomic effect across HDF and iPS cells (**Fig. S9b, Table S6**).

Next, we extracted the significant differential active molecular features of the 33 lncRNAs from both studies (**Fig. S9c**). We showed that the same-target-ASO-pairs are more concordant than the different-target background for genes and pathways even across HDF and iPS cells (**Fig. S9d**), however, common motifs are not found under the current cutoffs. To define lncRNAs showing consistent molecular phenotype across HDF and iPS cells, we required concordant ASO-pairs with at least one common active molecular feature. This resulted in 36 ASO-pairs targeting 22 lncRNAs (**Fig. 6d-e**). Furthermore, the common differentially active genes and pathways among these 22 lncRNAs are mostly different (**Fig. S9e**), excluding the possibility of non-specific side effects as a contributing factor for the observed concordance.

At the molecular level, knockdown of *TUG1* suppresses the expression of *ASCC2* in both HDF and iPS cells while Hi-C contact between these two genes were found in both cell-types (**Fig. S9f**). Another example is the knockdown of *SPRY4-AS1* in regulating *ARHGAP26* with significant Hi-C contacts in both cell-types (**Fig. S9g**). Further, the knockdown of *KHDC1-AS1* was categorized as non-concordant between HDF and iPS cells as different ASOs KD samples were subjected to CAGE. We tested the whole panel of ASOs in iPSC again in RT-qPCR and found the *cis*-regulated *KCNQ5* in HDF[8] was also suppressed by the knockdown of *KHDC1-AS1* in iPS cells (**Fig. S9h**). This suggested different ASOs may target different isoforms and potentially the molecular concordant events may be under-estimated.

Discussion

We devised a systematic workflow to functionally characterize 202 lncRNAs in human iPS cells through both cellular and molecular phenotyping upon ASO-mediated knockdown. The large-scale perturbation study has revealed a scalable and effective way to evaluate their functional roles and primary targets in iPS cells. Here, we annotated 34 lncRNAs affecting cell growth and 36 lncRNAs that elicit robust molecular features. The molecular phenotyping was extended to the identification of *cis*- and *trans*-acting lncRNAs and the identification of lncRNAs that affect stem cell identity.

We report that 18.3% of the lncRNAs exhibit a growth phenotype. This rate is comparable with our previous ASO array screen on human dermal fibroblasts[8] but higher than a CRISPRi pool screening which showed 5.9% of lncRNA loci affecting cell growth in human iPS cells.[17] Comparing the 65 common lncRNAs in the CRISPRi pool screening, we found few

overlaps between the two studies (**Fig. S2d-e**). The inconsistency could be partly due to the perturbation methods whereby CRISPRi targets DNA regulatory elements that may function independently from the RNA.[44,45] This study directly targets the RNA by using ASOs, thus, focusing on the transcripts alone and avoiding interference from promoter suppression. Other explanations could be due to the strategy of stable or transient suppression, iPS clone, method to measure cell growth, non-targeting control used, etc.

We found enhanced knockdown efficiency for lncRNAs with nuclear enrichment and higher expression levels when using LNA gapmer ASOs. It has been reported that ASOs mediate the degradation of nuclear RNA including nascent RNA effectively relying on the higher enrichment of endogenous RNase H1 in the nucleus.[46] This supports the knockdown of lncRNAs which are largely found to regulate genes epigenetically inside the nucleus.[6] LncRNAs expressed highly and ubiquitously across different cell-types were shown to affect cell growth (**Fig. 2h**). This suggests a set of ubiquitously expressed lncRNAs is indispensable and mediates common and essential pathways such as cell cycle progression, even though lncRNAs have been previously considered cell-type specific. It is possible that their cell-type specific roles may only be activated by specific stimulation such as differentiation.

Previous studies have highlighted that the same lncRNA expressed in two different cell-types might have distinct cellular functions.[17] Consistent with the study, we observed distinct cellular phenotypes exhibited by the same lncRNAs. However, we observed a high consistency in the molecular phenotype across both cell-types (**Fig. 6e**), suggesting the same molecular function of a lncRNA may affect the cell growth phenotype differently. Nevertheless, the concordant growth phenotype is generally under-estimated due to the insufficient knockdown, which may not affect molecular phenotyping when multiple genes from the transcriptome are considered. Therefore, screening solely relying on cell growth assays significantly underestimates functional classification of lncRNAs.

Integration analyses provide a platform to identify the primary targets of lncRNAs, many of which function at the epigenetic level. The enrichment analyses have highlighted two lncRNAs as master regulators, affecting the expression of multiple genes nearby. For instance, *LINC00240*, which was shown to promote cancer cell growth,[47] supports the expression of several histone genes in the nearby locus with significant Hi-C contacts and eQTL linkages (**Fig. 4a**). Besides, we highlighted the *cis*-regulatory role of *TUG1* in controlling *SELENOM*. This *cis*-regulation was also found in mouse after *Tug1* knockout,[48]

however, the direction of regulation of the *cis*-genes including *SELENOM* (*Selm*) and *MORC2* (*Morc2a*) are opposite to our findings (**Table S4**). In addition to species-specific lncRNA function, the distinct *cis*-responses may be caused by the different methods of perturbation. From the RNA-DNA-interactions, a canonical *trans*-regulator,[34] *FIRRE*, was also shown to support the expression of multiple interacting genes in the same and different chromosomes. While the exact dynamics to evaluate the cause-and-effect of lncRNA knockdown is still predictive, the integrative analysis provides an in-depth insight into potential regulatory processes for downstream analysis. A study including multiple time points will be useful for dissecting the precise dynamic mechanisms of lncRNA in the future.

In summary, our study outlined a robust high-throughput lncRNA-perturbation, real-time imaging and transcriptomic profiling in a systematic fashion. This platform identified lncRNAs with functional roles by cellular and molecular phenotyping in iPS cells. Additionally, lncRNAs which are commonly expressed across cell-types, were found to show similar molecular roles while the downstream cellular responses leading to growth phenotype vary. Integrating DNA-DNA and RNA-DNA interaction data with the knockdown CAGE profiles enhance the identification of primary gene targets of lncRNAs, shedding novel perspectives to elucidate their mechanistic roles in a global manner. The functional conservation and redundancy of lncRNAs will be better addressed when functional screening of lncRNA is performed in more cell-types.

Methods

Gene models, lncRNA target selection and ASO design

The gene models and gene classes (divergent, antisense and intergenic lncRNAs) were interpreted and defined by FANTOM CAGE Associated Transcriptome (CAT).[1] The selection of the 390 lncRNA targets cover different expression levels and different gene classes, while maintaining an expression level above 0.1 TPM according to the mean of three different iPS lines.[1] Selection was achieved by manually curating the loci suitable for ASO design (e.g. without overlapping other mRNAs on the same strand).

The strategy of the locked nucleic acid (LNA) phosphorothioate gapmer ASO design has been described previously.[8] Briefly, ASOs were designed with a central DNA gap flanked by 2-4 LNA nucleotides at the 5’ and 3’ ends of the ASOs. For each lncRNA target, we used the unspliced transcript sequence from FANTOM CAT as a template for designing a minimum

of 5 ASOs per lncRNA. An exhaustive list of all target recognition sequences of 16-19 nt in length within the unspliced target lncRNA sequence was analyzed against the entire transcriptome to determine the prevalence of each *k*-mer, when allowing for 0 or 1 mismatched positions. Furthermore, the accessibility of each *k*-mer in the target sequence was estimated using RNAplfold using the ViennaRNA package.[49] Subsequently, ASO designs were generated by applying various LNA/DNA design motifs to the reverse complement of the *k*-mer sequences. The LNA/DNA design patterns consisted of any combination of 2-4 LNA modifications at the 5' and 3' ends and central DNA window. For each ASO design, we calculated a series of characteristics, including predicted melting temperature for the ASO:RNA duplex, presence of problematic sequence motifs (G-quadruplex and other homopolymers, 5' terminal GG) as well as propensity to fold/co-fold estimated by using RNAfold and RNAcofold (ViennaRNA package) on the ASO sequence. Finally, ASOs were selected based on properties of both the *k*-mer binding site in the target lncRNA sequence and characteristics of the different ASO designs, such that ASOs had zero perfectly matched off-targets, and no more than 1 imperfectly matched off-target, when allowing for 1 mismatched position. In addition, ASOs were selected to have a predicted melting temperature (T_m) in the range of 50-56°C.[50] A total of 2,225 ASOs targeting 390 lncRNAs were selected for the study. The ASOs were synthesized by Exiqon (1,923 ASOs) and GeneDesign Inc. (302 ASOs).

Cell culture

Human induced pluripotent stem (iPS) cells were generated by infecting human dermal fibroblast-fetal (HDF-f, Cell Applications INC.) with a non-integrating Sendai-based viral vector (SeV) coding for OCT3/4, SOX2, KLF4 and c-Myc, as described.[51] The iPS cells were cultured in StemFit medium (ReproCELL Inc., Yokohama, Japan) under feeder-free conditions at 37°C in a 5% CO_2 incubator. The cells were plated on a culture dish pre-coated with laminin-511 (iMatrix-511: Nippi, Tokyo, Japan). Rho-associated kinase (ROCK) inhibitor, Y-27632 (Wako Pure Chemical Industries Ltd., Osaka, Japan) was added to the cells at a final concentration of 10 μM during the first 24 h of incubation after plating. StemFit medium is refreshed daily until the next passage. The cells were dissociated and detached by incubating with TrypLE select (Thermo Fisher Scientific) followed by scraping in StemFit medium. The cell viability in each passage is > 95%, as monitored by a trypan blue exclusion assay. For spontaneous differentiation conditions, FGF2 was removed from the complete medium 24 h after plating the cells.

Human dermal fibroblasts (HDFs) used were primary cells derived from the dermis of normal human neonatal foreskin cells (Lonza, catalog number: C2509). The cells were cultured in Dulbecco's Modified Eagle's medium (high glucose with L-glutamine) supplemented with 10% fetal bovine serum at 37°C in a 5% CO_2 incubator. The passage number of the cells for transfection was maintained at six or seven.

Transfection

The iPS cells were transfected in a 96-well plate. The cells were seeded 24 h before transfection at a density of 7,200 cells per well. A final concentration of 20 nM siRNA (Thermo Fisher Scientific) or ASO, and 0.2 µL lipofectamine RNAiMAX (Thermo Fisher Scientific) was mixed in 20 µL OptiMEM (Thermo Fisher Scientific). These transfection reagents were incubated at room temperature for 10 min and mixed with 90 µL StemFit medium without ROCK inhibitor. The medium from the 96-well plate was aspirated and replaced with the transfection mix. The volume and cell number were scaled in proportion if other sizes of well were used. The whole screening included 2225 ASOs (390 lncRNA targets) in duplicate. Each 96-well plate included 2 wells for mock transfection (lipofectamine alone), 4 for non-targeting negative control (NC, Exiqon) and 2 for ASO targeting *MALAT-1* (MA-1, Exiqon) to control knockdown efficiency. For the transfection for HT-CAGE screening, 317 ASOs (123 lncRNA targets) were selected according to knockdown efficiency and growth phenotype in the screening. They were transfected with duplicates, in parallel with 4 untreated samples, 20 mock transfections, 48 NC and 8 MA-1. Several ASOs targeting characterized genes including *POU5F1*, *LncRNA-ES1*, *LncRNA-ES3*, and siRNAs targeting *POU5F1* and *EMC7* were also included as positive controls. The sequences of ASOs and siRNAs used in this study were listed in **Table S7**.

Real-time imaging

Phase-contrast images of transfected cells were captured every 3 h for 2 days with 4 fields per well by the IncuCyte live-cell imaging system (Essen Bioscience). The confluence in each field was analyzed by the IncuCyte software. The mean confluence of each well was taken from each time point starting from 15 h post-transfection until the mean confluence of the NC ASOs in the same plate reached 90%. The growth rate in each well was calculated as the slope of a linear regression. A normalized growth rate of each sample was calculated as the growth rate of the samples divided by the mean growth rate of the 4 NC ASOs from the same plate. Student's *t*-test was performed between the growth rate of the duplicated samples and

the 4 NC ASOs, assuming equal variance. Transfection of an ASO was considered to inhibit growth if the normalized growth rate < 0.63 (6 standard deviations from the mean normalized growth rate of NC) and *t*-test *p*-value < 0.05 (comparison between sample and NC).

RNA purification

The harvested lysates were subjected to purification using the RNeasy 96 Kit (Qiagen) and epMotion automated liquid handling systems (Eppendorf) according to the manufacturers' instructions. The eluted RNA was quantified by the NanoDrop™ spectrophotometry platform (Thermo Fisher Scientific). The purified RNA samples were stored at -80 °C until they were used for the RT-qPCR assay or the HT-CAGE library construction.

Real-time quantitative RT-PCR

Real-time quantitative RT-PCR was performed by One Step PrimeScript™ RT-PCR Kit (Takara Bio Inc.) using the epMotion automated liquid handling system (Eppendorf). For each lncRNA target, 3 primer pairs against the specific lncRNA target were used. The expression level was normalized by *GAPDH* while the knockdown efficiency was calculated from the fold-change between specific samples and the transfection of NC ASOs. The knockdown efficiency of *MALAT1* was monitored along each run and across all the runs where all the samples have >90% KD. The primers' sequences are listed in **Table S7**.

WST-1 growth assay

Cells were transfected in a 96-well format as described above. At 48 h post-transfection, the medium was discarded and replaced with 100 µL StemFit medium and 10 µL WST-1 solution (Abcam). The cells were incubated at 37°C in a 5% CO_2 incubator for 1 h, followed by measurement of OD 450 in a microplate reader. All absorbance values were subtracted by the control value from empty wells containing 100 µL StemFit medium and 10 µL WST-1 solution. These subtracted absorbance values were further normalized by cells transfected with NC ASOs seeded on the same plate. This batch of transfection included 317 ASOs selected for HT-CAGE. These transfected cells have real-time imaging measurement in parallel.

Colony formation assay

Reverse transfection was used for this assay. The cells were incubated with ROCK inhibitor in complete StemFit medium for 1 h before detachment by Accutase. After detachment, cells

were centrifuged and resuspended in StemFit medium. Transfection mix was prepared as a 200 µL solution containing 2 µL lipofectamine RNAiMAX and 20 nM siRNA / ASO in the StemFit medium. The mix was maintained at room temperature for 10 min, followed by addition of 10,000 cells in 200 µL StemFit medium. After 15 min, 3,000 cells in 0.5 mL StemFit medium were seeded onto a 24-well pre-coated with laminin-511. Cells were refreshed after 3 days and stained by 0.5% crystal violet at day 6. The wells were imaged by the Celigo Image Cytometer (Nexcelom Bioscience) and the number of colonies were counted by ImageJ.[52]

High-throughput low quantity cap analysis of gene expression (HT-CAGE)

We selected 317 ASO knockdown samples from 123 lncRNA targets for HT-CAGE analysis. The selection was done by manual curation where we selected ASOs with relatively similar knockdown efficiency, where 301 are effective ASOs and 16 of them show marginal knockdown efficiency (> 40% in general). Among the 123 lncRNAs, 20 show growth phenotype from the cellular phenotyping. In parallel, NC ASOs, negative non-targeting control and positive controls such as ASO and siRNA targeting *POU5F1* were also subjected for HT-CAGE.

Fifty nanogram of purified RNA was used from each sample, which was 96-multiplexed for constructing one single-strand CAGE library,[22] according to an improved version of nAnT-iCAGE protocol[21] that avoids any bias from PCR amplification. Libraries were subjected to 50-base pair-end sequencing using an Illumina HiSeq 2500 instrument. Tags were de-multiplexed and mapped to the human genome (hg38) using STAR.[53] The median number of mapped CAGE transcription start sites (CTSS) obtained from each sample is about 500,000. Gene expression profile was analyzed by intersecting the mapped CTSS with the permissive CAGE peaks regions (of 709,716 promoters) annotated in FANTOM CAT.[1] Promoter-level expression profiles were used in motif activity response analysis (MARA). Gene-level expression profiles were aggregated from promoter-level profiles for other downstream analyses.

HT-CAGE allows samples to be highly-multiplexed by introducing additional barcodes in the RT primer,[22] which is ideal for large-scale perturbation studies. From the *POU5F1* knockdown using either ASO or siRNA, we compared the performance of standard nAnTi-CAGE[21] with HT-CAGE, which resulted in less sequencing reads (**Fig. S10a**). The transcriptomic profiles after the knockdown suggested that HT-CAGE and standard CAGE

are highly concordant (*rho* = 0.695, **Fig. S10b**). Although the knockdown efficiency of ASOs was generally lower (**Fig. S10c**), the transcriptomes between ASO and siRNA knockdown remained highly reproducible (**Fig. S10b**). The results of Gene Set Enrichment Analysis (GSEA) (**Fig. S10d**) also showed that the perturbed samples were clustered by oligos and not by technologies or modalities (**Fig. S10e**).

Global analysis of cellular phenotype of same-target ASOs

From 2,225 ASOs, 756 ASOs showed effective knockdown (knockdown efficiency > 50% in one of the 3 primer sets) while 1469 of them were considered without effective knockdown. The one-way ANOVA test was carried out on the 202 lncRNAs targets from 686 ASOs, with 2-10 successful ASOs per target, using the normalized growth rate for each ASO and gave the *p*-value = 2.79×10^{-5} (**Fig. 2e**). The analysis was done in R 4.0 using the 'aov' function ('*stats*' 4.1.1 package) and the target labels were permuted using the 'shuffle' function ('*mosaic*' 1.8.3 package).

Growth phenotype determination of lncRNA target

At a robust level, lncRNAs with ≥ 2 independent effective ASOs resulted as growth inhibition (normalized growth rate < 0.63, t.test *p*-value < 0.05) are considered as showing growth phenotype (37/202). To implement a stringent level with statistical correction, we applied binomial and required *p*-value < 0.05 as a stringent cutoff. From the 2,225 ASOs, 1,469 of them were considered without effective knockdown. We set these 1,469 ASOs as the background to represent the maximum possible chance of growth inhibition mediated by side effects. The rate of significant growth inhibition from the background and for the effective ASOs is 15.1% and 23.5%, respectively. Since the number of successful knockdown ASOs for each lncRNA is different, we set up a binomial test to assess how many ASOs showing growth inhibition is significantly higher than background (binomial *p*-value < 0.05). Briefly, we have taken 15.1% as background growth inhibition, with the chance of ≥ 2 ASOs in the group of lncRNA with 2 ASOs showing successful knockdown is $0.151^2 = 0.022801$, which means that a false positive occurring randomly is < 5%. We set a conditional cutoff for different groups of lncRNA having different numbers of successful knockdown ASO to keep the chance of false positives lower than 5%. Using this stringent cutoff, 12 lncRNAs were considered to have a growth phenotype.

Correlation between gene properties and growth phenotype

These analyses were done target-based. LncRNAs were grouped as successful knockdowns if ≥ 2 ASOs showed reduction of the specific RNA level by 50%, considering the primer set showing the strongest knockdown result from the RT-qPCR. By this criterion, 202 lncRNAs were grouped as successful knockdown and 188 were grouped as no KD. From the 202 lncRNAs, 37 of them were grouped as growth phenotypes where ≥ 2 ASOs showed reduced normalized growth rate compared to that of the NC ASOs significantly with a cutoff of smaller than 0.63 (6 standard deviations from the mean of NC). The 165 lncRNAs were grouped as having no growth phenotype. The tests were performed between successful knockdown (n=202) and no knockdown (n=188), and between growth phenotype (n=37) and no growth phenotype (n=165). Discrete gene properties, including derived from promoter or enhancer, intergenic or non-intergenic, antisense or non-antisense, divergent or non-divergent, were accessed by Fisher's exact one-tailed test. Gene properties with continuous values were analyzed by the Wilcoxon one-tailed test. The transcription initiation regions (TIR) and exon conservation scores were derived by rejected substitution scores as described.[1] Exosome sensitivity score was derived from comparing the transcriptome of control and EXOSC3 knockdown in our iPS line using the formula ($TPM_{Exosome\text{-}suppressed}$ - $TPM_{Control}$) / $TPM_{Exosome\text{-}suppressed}$.[54] Expression levels of the targets were revealed from CAGE sequencing and RNA-seq data of our iPS line. The number of exons refers to the maximum number of exons from any transcripts of the lncRNAs. Cell-type specificity (Gini index calculated from 71 cell-types in FANTOM5) is described in the corresponding methods. The number of Hi-C contacted eQTL-contacted and RADICL contacted protein-coding genes with TPM > 0.1 are identified as described in the corresponding methods. Comparison based on growth phenotype with stringent cutoff (12 VS 190) and molecular phenotype (36 VS 87) are shown in **Table S2**. The Wilcoxon tests were done in R 4.0 using the wilcox.test function ('*stats*' 4.1.1 package).

Motif Activity Response Analysis (MARA)

MARA[55] was performed using TMM normalized and batch corrected promoter expression profiles for all the ASO knockdown and controls (NC ASOs and other positive controls) libraries (732 CAGE libraries). Batch correction was performed by the "removeBatchEffect" function in the limma R package. All promoters with expression ≥ 1 TPM at least in 70% CAGE libraries (13,883 promoters) were used for the analysis. Transcription factor binding

sites (TFBS) for hg38 were predicted as described previously[56] using MotEvo[57] for the set of 190 position-weight matrix motifs in SwissRegulon (released on 13 July 2015)[58] on a multiple alignment of genome assemblies. The number of predicted TFBS were counted for each motif in the -300 to +100 base pair from the midpoint of the FANTOM CAT promoters. Next, MARA was performed to decompose CAGE expression profiles of the promoters in terms of their associated motifs, yielding the activity profile of all the motifs with at least 150 TFBS associated with the expressed promoters across the iPS cells knockdown and control samples. The comparison was done by 2 knockdown libraries per ASO versus 47 libraries of NC ASOs by using the Wilcoxon test for the *p*-value, which was adjusted by the Benjamini-Hochberg method. Net activity was calculated by the mean activity of each ASO minus the mean activity of the 47 NC ASOs. The motifs showing FDR < 0.1 were considered significant. The MARA results per ASO are listed in **Table S8**.

Differential expression

Differential expression of 10,868 genes was performed by *edgeR* (ver. 3.10)[59] after aggregating the promoter-level profiles. A design of 2 libraries of ASO versus 47 libraries of NC using TMM normalization was adopted after batch effect correction. FDR was obtained by p.adjust from the p-value of *edgeR* using the Benjamini-Hochberg method. Across sample Z-score was calculated from the $\log_2$FC of a gene across the 317 ASO knockdown samples. The genes showing FDR < 0.1 and |Z-score| > 1.645 were considered as significant changes for downstream analyses. The raw count and the TMM-normalized count per gene (n = 10,868) per library (n = 732) will be deposited to a public repository and be visualized in the Zenbu genome browser (https://fantom.gsc.riken.jp/zenbu/). The *edgeR* results per gene (n = 10,868) per ASO (n = 317) are listed in **Table S9**.

Gene set enrichment analysis (GSEA) for cellular pathways

Gene set enrichment (GO Biological Process, GO Molecular Function, GO Cellular Component, KEGG, Hallmark and Reactome) analysis was carried separately for each set of pathways and each ASO knockdown using '*fgsea*' (1.8.0) R-package[60] with the following parameters: minSize=15, maxSize=1000, nperm=10000, nproc=1. Each pathway was tested using gene ranks based on $-\log_{10}$(*p*-value) × sign($\log_2$FC) from the *edgeR* analysis. Across samples, the Z-score was obtained by NES dividing into positive values and negative values from the 317 ASO samples. Pathway was considered significant if adjusted *p*-value < 0.05 and |Z-score| > 1.645. The GSEA results per ASO are listed in **Table S10**.

Concordance test of molecular phenotype by same-target-ASO-pairs

We selected 123 lncRNAs (317 ASOs) for HT-CAGE sequencing. These 317 ASOs were paired for targeting the same lncRNAs and resulted in 293 same-target-ASO-pairs, which were then shuffled and enforced into different-target-ASO-pairs, 10,000 times for permutation.

Here, we use the *edgeR* results as an example. To determine if ASO knockdown resulted in a specific effect stronger than noise (effects of ASO transfection), we used the Jaccard index of common significant DEG in the same direction to quantify the degree of concordance between two ASOs in a pair. Briefly, differentially expressed genes (excluded the target lncRNAs) from each ASO-knockdown were taken with FDR < 0.1 and |Z-score| > 1.645. From the 293 ASO-pairs, the mean Jaccard index was calculated for the same-target group. The mean values for each permutation of the different-target group were calculated to generate a distribution. The empirical *p*-value represents the chance that the mean values of the same target group is not greater than the different-target group. For all the tested conditions using the Jaccard index in *edgeR*, the empirical *p*-values are < 0.0001.

Degree of transcriptome change predicts growth phenotype

The 317 ASO knockdown profiles from *edgeR* were compared with the NC ASO-background by their $-\log_{10}$(*p*-value) of all the 10,868 genes. Briefly, a KS curve was plotted for each knockdown profile to calculate the mean distance between one ASO and the NC-background. Each NC-ASO-combination was also compared with the NC-background. Next, ASOs were paired if targeting the same lncRNA. The calculated distances of the two ASOs were compared with distances of 47 NC ASOs by the Wilcoxon test. The *p*-values from the tests were adjusted by the Benjamini-Hochberg method across all the ASO-pairs for FDR. The mean distance of the 2 ASOs and the $-\log_{10}$(Wilcoxon *p*-value) were plotted in the chart (**Fig. 3a**).

Correlation between GSEA pathways and cellular phenotype

From the *fgsea* result, we extracted the $-\log_{10}$(adjusted *p*-value) × sign(NES) of the 317 ASOs for each pathway. These values were compared with the normalized growth rate of the 317 ASOs by Spearman correlation for each pathway. The rho values for all the pathways are reported in **Figure 3b**.

Identification of concordant ASO-pairs from the same lncRNA targets

After showing same-target ASO-pairs are more concordant then different-target ASO-pairs from the results of *edgeR*, pathway GSEA and MARA, we performed an additional enrichment test to identify concordant ASO-pairs, which imply a hit of molecular phenotype at the lncRNA level. The method of the enrichment is illustrated in **Fig. S4a-c**. Briefly, we rank the knockdown profile for each ASO using $-\log_{10}$(p-value) × sign($\log_2$FC) from *edgeR*. The top and bottom 25, 50, 75, 100, 125, 150, 175 and 200 genes were taken as genesets. These genesets for all the 317 ASOs were tested for enrichment against all the knockdown profiles of the 317 ASOs by '*fgsea*' (1.8.0) where each geneset size was tested separately for the adjusted *p*-values. The NES values of the different-target-ASO-pairs were scaled for a normalized background distribution. An same-target-ASO-pair was considered significant if both the forward test and the reverse test adjusted *p*-values < 0.05 with |NES Z-score| > 1.645. Either positive and negative enrichment was considered a hit. The hits were called from the union of any of the geneset sizes (**Fig. 3c**).

Optimal cutoffs of molecular features

To improve the performance, we attempted to apply two types of background correction, NC-background correction and across sample (317 ASOs) background correction. For the NC-background, maximum combinations of two libraries from 47 NC ASOs CAGE libraries were obtained. These 1,081 NC combinations were applied to *edgeR*, *fgsea* and MARA analysis similarly as the ASO samples. The resulting $\log_2$FC, NES and motif activity values of these 1,081 combinations were scaled as normalized backgrounds. For the across sample background, $\log_2$FC, NES and motif activity from the 317 ASO samples were scaled as normalized background. The transformed Z-score of the actual values were used as background correction using |Z-score| > 1.645 as a cutoff.

After the assessments by using Jaccard indices (**Fig. S4f**), all the tested conditions in all the molecular features revealed the same-target-ASO-pairs are more concordant than the different-target background significantly (empirical *p*-values are < 0.0001). We selected the best cutoffs by maximizing the ratio of concordance of same-target-ASO-pairs to different-target-ASO-pairs, resulted in FDR < 0.1 with |across-sample Z-score| > 1.645 for genes (*edgeR* analysis), adjusted *p*-value < 0.05 with |across-sample Z-score| > 1.645 for pathways (*fgsea* analysis) and FDR < 0.1 for motifs (MARA analysis).

Cell-type specificity on expression level

FANTOM 5 CAGE data on ~120K genes with 384 samples with cell ontology classification[54] plus iPS and ES cells (iPS in this study was not included) were used to determine cell-type specificity for all the RNA including the lncRNA targets. CAGE libraries used were listed in Table S5. We applied the Gini index for each gene from the RLE normalized TPM across the 71 cell-types. To compare cell-type specificity between mRNA and lncRNA, genes were grouped by the maximum TPM across the 71 cell-types. Gene annotation of mRNA and lncRNA was according to the FANTOM CAT gene classes.[1] Statistical significance in each group was acquired by applying the Student's *t*-test where *p*-value < 0.05 was considered significant in **Figure 6a**.

For building a geneset for the 71 cell-types for cell-type enrichment analysis, expression levels of a gene in a cell-type lower than 5% of the maximum TPM were considered as lack of expression, and the corresponding Gini index set as 0. Only including the 10,868 genes detected from HT-CAGE, the top 25, 50, 75, 100, 125, 150, 175 and 200 genes ranked by the Gini index were taken for each cell-type. These genesets for 71 cell-types were tested for enrichment against all the knockdown profiles of the 317 ASOs by '*fgsea*' (1.8.0) where each geneset size was tested separately for the adjusted *p*-values. The NES values across the 317 ASOs were scaled and cross-samples Z-scores were obtained. LncRNA targets having at least 2 ASOs with adjusted *p*-value < 0.05 and |Z-score| > 1.645 towards a cell-type were considered significant. A list of significant lncRNA targets was obtained from the union of the 8 geneset sizes.

Cell fractionation for RNA-sequencing

Subcellular fractionation of native iPS cells was performed similarly as HDF as previously described[8] with minor optimization according to the cell-type. Briefly, approximately 10 million cells were used per fractionation experiment to obtain cytoplasmic (CYTO), soluble nucleoplasmic (SNUC) and chromatin (CHR) fractions. Trypsinized cells were washed and lysed using a cold lysis buffer containing 0.15% Igepal CA-630, 10 mM Tris pH 7.5, 150 mM NaCl. The lysate was centrifuged in a sucrose cushion, after which the supernatant was taken as the CYTO fraction. The nuclear pellet was washed once in a buffer containing 20 mM HEPES pH 7.5, 50% glycerol, 75 mM NaCl, 1 mM DTT, 0.5 mM EDTA and resuspended in the same buffer. An equal volume of nuclear lysis buffer containing 20 mM HEPES pH 7.5, 300 mM NaCl, 1M Urea, 1% Igepal CA-630, 10 mM $MgCl_2$, 1 mM DTT,

0.2 mM EDTA was added and incubated on ice for 5 min. After centrifugation, the supernatant was considered as the SNUC fraction and the pellet as the CHR fraction. The chromatin pellet was washed once in a buffer containing 10 mM HEPES pH 7.5, 10 mM KCl, 10% glycerol, 340 mM sucrose, 4 mM $MgCl_2$, 1 mM DTT and resuspended in the same buffer. RNA from each fraction was isolated using Trizol LS (Invitrogen), according to the manufacturer's instructions. Next, DNase I treatment followed by phenol-chloroform extraction was conducted. The volume and concentration of the RNA isolated from each fraction was recorded, with an equal amount of RNA for each fraction was used for RNA-sequencing.

Single-end read RNA-sequencing was performed with the Illumina platform by HiSeq2000. Fastq data were mapped towards human genome assembly GRCh38 (hg38) and FANTOM CAT permissive transcript model[1] using TopHat2.[61] The resulting gene length and library size normalized tpm values in each fraction were multiplied by the corresponding RNA content factors (amount of RNA extracted from each fraction divided by the sum of the RNA amount of all fractions). The fraction-normalized tpm (nTPM) was used to calculate the nucleus ratio from the whole cell ((SNUCnTPM + CHRnTPM) / (CYTOnTPM + SNUCnTPM + CHRnTPM)) and the chromatin ratio from the whole nucleus (CHRnTPM / (SNUCnTPM + CHRnTPM)).

The median value of the nucleus / whole cell ratio was calculated from all the genes with >1 TPM in iPSC (as 0.1418). Targets with the nucleus ratio smaller than this were considered as cytoplasmic-enriched. The remaining targets were grouped as chromatin-enriched for their chromatin / whole nucleus ratio greater than the median. The remaining targets are soluble nucleoplasmic enriched.

Concordant knockdown responses between HDF and iPS cells

The knockdown profiles by individual ASO in iPS cells were generated by *edgeR* as earlier described. The knockdown profiles in HDF cells were obtained by DESeq2[62] after nAnTi-CAGE sequencing, as described previously.[8] Only genes (n=10,054) overlapping in both analyses were included, with these genes ranked by $-\log_{10}(p\text{-value}) \times \text{sign}(\log_2 FC)$. Genesets with sizes of 25, 50, 75, 100, 125, 150, 175 and 200 were generated from each ASO knockdown profile from the top and the bottom of the ranking. Gene sets were tested for enrichment by '*fgsea*' (1.8.0) in the knockdown profiles of the ASO with the same targets in the other cell-type. Enrichment tests were also performed towards the knockdown profiles

from the different-target-ASO-pairs (n = 250, 10,000 permutation) to build the background. In total, 250 different-cell-types-same-target-ASO-pairs were tested and significant pairs meet the following criteria in either up-/down-regulation in any geneset size: both forward and reverse enrichment adjusted *p*-values < 0.05 while both forward and reverse |different-target different-cell ASO-pairs background Z-score| > 1.645.

For the common significant molecular features applied to each same-target-ASO-pair, we used the same cutoffs defined above for iPS cells. For HDF, we used FDR<0.01, $|\log_2 FC|$ > 0.5 and |Z-score|>1.645 for genes; adjusted *p*-value < 0.05, |NES|>1 and |Z-score|>1.645 for pathways; FDR<0.05 and |Z-score|>1.645 for motifs. The target lncRNAs were excluded from the common differentially expressed genes.

Hi-C

The experimental setup of Hi-C for iPS cells is the same as HDF cells, as described previously.[8] The analytical pipeline has been described.[26] Briefly, after the binomial test at 10 kb resolution for intra-chromosomal interactions, respectively, interacting regions with FDR < 0.05 were considered significant. The bin regions were intersected with the whole gene regions (gene region + 800 bp upstream the transcription start site) of the lncRNA targets, the whole gene regions of mRNAs and the promoter regions of mRNAs (800 bp upstream and 200 bp downstream of the transcription start site of all transcripts) defined in FANTOM CAT.[1] The whole gene region against whole gene region interaction was used to identify contacted protein-coding genes of the lncRNA targets. We used the contacted protein-coding genes that are detectable in HT-CAGE to construct genesets for enrichment analysis against the knockdown profiles of each ASO by '*fgsea*' (1.8.0). The whole gene region of lncRNA against the promoter region of mRNA interaction was used as an extra indicator of regulation. The TAD regions in the whole genome of iPS cells were predicted by the Hi-C data at 50 kb resolution, as described previously.[26] Inter-chromosomal Hi-C interactions was identified at 50 kb resolution and mapped to genes the same way as intra-chromosomal interactions. The inter-chromosomal Hi-C interaction was only used to filter RADICL inter-chromosomal signal. However, there were only 62 lncRNA-protein-coding genes inter-chromosomal Hi-C pairs identified and they did not overlap with any RADICL signals.

Expression quantitative trait loci (eQTLs)

The eQTL-linked genes were obtained from the Genotype-Tissue Expression (GTEx) project (v8).[27] The eGene and significant variant-gene associations based on permutations were taken from 49 tissues with the permutation *q*-value < 0.25. The genomic location of the genetic variants was intersected with the 390 lncRNA targets for their whole gene region (gene region + 800 bp upstream the transcription start site). For the eGenes, only protein-coding genes having expression with at least 0.1 TPM from iPS cells or being detected by HT-CAGE were included.

RADICL-seq

RNA And DNA Interacting Complexes Ligated and sequenced (RADICL-seq) was performed, as described previously.[24] The analytical pipeline was performed as described previously[26] with modification. Briefly, RNA mapped to a defined set of small RNAs was removed from the dataset. The genome was then divided into 25 kb bins and the annotated RNA reads were aggregated. The background probability for a bin was calculated by dividing the count of trans mRNA binding in that bin by the total number of trans mRNA reads. To estimate the significance of binding each gene in every bin, we performed a one-sided binomial test using binom_test (x,n,p) from scipy where x = the number of reads for the gene in the bin; n = total number of reads for the gene; p = background probability calculated using trans-binding mRNA in the bin. FDR was obtained by p.adjust from the binomial *p*-values using the Benjamini-Hochberg method across all the bins per RNA. The regions with at least 3 reads and FDR < 0.05 were considered significant. The regions from the DNA side were intersected towards the whole gene regions (gene region + 800 bp upstream the starting site) of mRNAs and the promoter regions of mRNAs (800 bp upstream and 200 bp downstream of the CTSS of all transcripts) defined in FANTOM CAT.[1] The RADICL-contacted protein-coding genes for each of the lncRNA target were taken if the mRNA expressed higher than 0.1 TPM in iPS cells or being detected in HT-CAGE. RADICL-contacted genes with the minimum genomic distance greater than 1 Mb and without significant Hi-C interaction (intra- and inter-chromosomal) were defined as *trans*-interaction. These mRNAs taken for each of the 64 lncRNAs were used as genesets and tested against the knockdown profiles of 149 ASOs. In the individual pair analysis, the most significant regions were used to represent the mRNA if there were more than one region overlap with the gene body.

Global enrichment of contact and significant DEGs

123 lncRNAs were paired with 9974 protein-coding genes that are detectable in HT-CAGE in iPS cells. For all these pairs we extracted the *edgeR* results of the most significant ASO to define significant DEGs, and compare this to the presence of *cis*-interactions and trans-interactions. We only used the pairs derived from the 121 lncRNAs showing at least one *cis*-interaction and the 57 lncRNAs showing at least one *trans*-interaction (no significant Hi-C contact and at least 1 Mb genomic distance) for the respective tests. Fisher's exact one-tailed test was performed.

RNA-DNA sequence complementary analysis

The transcript models with the highest expression in the soluble nuclear fraction were used to represent the sequence of the lncRNA targets. These RNA sequences were mapped with the whole gene regions and the promoter regions of the RADICL-contacted mRNA using a window size of 20 bp allowing 20% mismatch. The mapping was done by the TDF software.[63] Any interaction with the whole gene regions (gene region + 800 bp upstream the starting site) of mRNA located > 1 Mb from the lncRNA gene region was counted.

Enrichment analyses between knockdown profile and contacts

The enrichment tests of protein-coding genes showing Hi-C contacts, RADICL-seq contacts and eQTL linkages with any of the 123 lncRNA targets with CAGE data were performed with '*fgsea*' (1.8.0) R-package.[60] The ~10,000 genes were ranked according to the $-\log_{10}(p\text{-value}) \times \text{sign}(\log_2 FC)$ from the *EdgeR* analysis of each ASO, which showed connected protein-coding genes in Hi-C, RADICL-seq or eQTL. The *p*-values were then the *p*-value adjusted by the Benjamini-Hochberg method. Inclusion criteria of protein-coding genes for Hi-C contacts: q-value < 0.05; RADICL-seq contacts: q-value < 0.05, read>=3; eQTL linkages: q-value < 0.25.

Acknowledgement

We thank Dr. Daisuke Yamada and Dr. Haruhiko Koseki for the generation of the iPS line. We also thank the Laboratory for Comprehensive Genomic Analysis in RIKEN for performing the next generation sequencing in this study. FANTOM6 was made possible by a Research Grant for RIKEN Center for Life Science Technology, Division of Genomic

Technologies (CLST DGT) and RIKEN Center for Integrative Medical Sciences (IMS) from MEXT, Japan.

Author's contribution

Conceptualization: C.W.Y., J.W.S.; Investigation: C.W.Y., C.H., K. Yasuzawa, D.M.S., J.A.R., Y.S., S.A, A.V.P., C.P.; Experimental analysis: C.W.Y., K. Yasuzawa, D.M.S., Y.S., A.V.P., C.P., Y.J.L., F.L., T.K., J.D., H.N., M.I., J.L., M.K., M.M., W.H.Y.; Computational analysis: C.W.Y., C.H., J.A.R., S.A, J.C., M.T., M.d.H., X.S.; Database management: I.A., A.H., T.K.; Genome browser visualization: J.S.; Writing (original draft): C.W.Y., J.W.S.; Writing (review & editing): C.H., D.M.S., J.A.R., Y.S., S.A, A.V.P., C.P., M.d.H., P.C.; Project supervision: C.W.Y., C.H., H.S., K.Yagi, T.K., M.d.H., P.C., J.W.S.; Funding acquisition: P.C.; Project administration: C.H., H.S., K.Yagi, T.K., M.d.H., P.C., J.W.S.

Supplementary Table

Table S1: Results of knockdown and growth phenotype

Table S2: Properties of 390 lncRNAs

Table S3: ASO-pair-base and lncRNA-target-base molecular phenotype

Table S4: Integration of Hi-C, RADICL-seq and eQTL to knockdown effects

Table S5: LncRNAs in cell identities

Table S6: LncRNA activities in HDF and iPS cells

Table S7: Sequences of ASOs, siRNAs and primers

Table S8: ASO-based results of *edgeR*

Table S9: ASO-based results of *fgsea*

Table S10: ASO-based results of MARA

References

1. Hon, C.-C. *et al.* An atlas of human long non-coding RNAs with accurate 5' ends. *Nature* **543**, 199–204 (2017).

2. Iyer, M. K. *et al.* The landscape of long noncoding RNAs in the human transcriptome. *Nat. Genet.* **47**, 199–208 (2015).

3. Guttman, M. *et al.* Chromatin signature reveals over a thousand highly conserved large non-coding RNAs in mammals. *Nature* **458**, 223–227 (2009).

4. Yao, R.-W., Wang, Y. & Chen, L.-L. Cellular functions of long noncoding RNAs. *Nat. Cell Biol.* **21**, 542–551 (2019).

5. de Hoon, M., Shin, J. W. & Carninci, P. Paradigm shifts in genomics through the FANTOM projects. *Mamm. Genome Off. J. Int. Mamm. Genome Soc.* **26**, 391–402 (2015).

6. Ma, L. *et al.* LncBook: a curated knowledgebase of human long non-coding RNAs. *Nucleic Acids Res*. **47**, D128–D134 (2019).

7. Palazzo, A. F. & Koonin, E. V. Functional Long Non-coding RNAs Evolve from Junk Transcripts. *Cell* **183**, 1151–1161 (2020).

8. Ramilowski, J. A. *et al.* Functional annotation of human long noncoding RNAs via molecular phenotyping. *Genome Res.* **30**, 1060–1072 (2020).

9. Takahashi, K. *et al.* Induction of pluripotent stem cells from adult human fibroblasts by defined factors. *Cell* **131**, 861–872 (2007).

10. Carcamo-Orive, I. *et al.* Analysis of Transcriptional Variability in a Large Human iPSC Library Reveals Genetic and Non-genetic Determinants of Heterogeneity. *Cell Stem Cell* **20**, 518-532.e9 (2017).

11. Fort, A., Yamada, D., Hashimoto, K., Koseki, H. & Carninci, P. Nuclear transcriptome profiling of induced pluripotent stem cells and embryonic stem cells identify non-coding loci resistant to reprogramming. *Cell Cycle Georget. Tex* **14**, 1148–1155 (2015).

12. Guo, C.-J. *et al.* Distinct Processing of lncRNAs Contributes to Non-conserved Functions in Stem Cells. *Cell* **181**, 621-636.e22 (2020).

13. Ng, S.-Y., Johnson, R. & Stanton, L. W. Human long non-coding RNAs promote pluripotency and neuronal differentiation by association with chromatin modifiers and transcription factors. *EMBO J.* **31**, 522–533 (2012).

14. Loewer, S. *et al.* Large intergenic non-coding RNA-RoR modulates reprogramming of human induced pluripotent stem cells. *Nat. Genet.* **42**, 1113–1117 (2010).

15. Wang, Y. *et al.* Endogenous miRNA sponge lincRNA-RoR regulates Oct4, Nanog, and Sox2 in human embryonic stem cell self-renewal. *Dev. Cell* **25**, 69–80 (2013).

16. Lin, N. *et al.* An evolutionarily conserved long noncoding RNA TUNA controls pluripotency and neural lineage commitment. *Mol. Cell* **53**, 1005–1019 (2014).

17. Liu, S. J. *et al.* CRISPRi-based genome-scale identification of functional long noncoding RNA loci in human cells. *Science* **355**, eaah7111 (2017).

18. Joung, J. *et al.* Genome-scale activation screen identifies a lncRNA locus regulating a gene neighbourhood. *Nature* **548**, 343–346 (2017).

19. Guttman, M. *et al.* lincRNAs act in the circuitry controlling pluripotency and differentiation. *Nature* **477**, 295–300 (2011).

20. Cabili, M. N. *et al.* Integrative annotation of human large intergenic noncoding RNAs reveals global properties and specific subclasses. *Genes Dev.* **25**, 1915–1927 (2011).

21. Murata, M. *et al.* Detecting expressed genes using CAGE. *Methods Mol. Biol. Clifton NJ* **1164**, 67–85 (2014).

22. Takahashi, H., Nishiyori-Sueki, H., Ramilowski, J. A., Itoh, M. & Carninci, P. Low Quantity Single Strand CAGE (LQ-ssCAGE) Maps Regulatory Enhancers and Promoters. *Methods Mol. Biol. Clifton NJ* **2351**, 67–90 (2021).

23. Marchese, F. P., Raimondi, I. & Huarte, M. The multidimensional mechanisms of long noncoding RNA function. *Genome Biol.* **18**, 206 (2017).

24. Bonetti, A. *et al.* RADICL-seq identifies general and cell type-specific principles of genome-wide RNA-chromatin interactions. *Nat. Commun.* **11**, 1018 (2020).

25. Li, X. *et al.* GRID-seq reveals the global RNA-chromatin interactome. *Nat. Biotechnol.* **35**, 940–950 (2017).

26. Agrawal, S. *et al.* Functional annotation of human long noncoding RNAs using chromatin conformation data. *bioRxiv* (2021) doi:10.1101/2021.01.13.426305.

27. GTEx Consortium *et al.* Genetic effects on gene expression across human tissues. *Nature* **550**, 204–213 (2017).

28. Dai, Q. *et al.* Long non-coding RNA TUG1 promotes cell progression in hepatocellular carcinoma via regulating miR-216b-5p/DLX2 axis. *Cancer Cell Int.* **20**, 8 (2020).

29. Guerriero, E. *et al.* Assessment of the Selenoprotein M (SELM) over-expression on human hepatocellular carcinoma tissues by immunohistochemistry. *Eur. J. Histochem. EJH* **58**, 2433 (2014).

30. Jiang, H. *et al.* Selenoprotein M stimulates the proliferative and metastatic capacities of renal cell carcinoma through activating the PI3K/AKT/mTOR pathway. *Cancer Med.* **8**, 4836–4844 (2019).

31. Liu, S., Yang, Y., Wang, W. & Pan, X. Long noncoding RNA TUG1 promotes cell proliferation and migration of renal cell carcinoma via regulation of YAP. *J. Cell. Biochem.* **119**, 9694–9706 (2018).

32. Pitts, M. W. *et al.* Deletion of selenoprotein M leads to obesity without cognitive deficits. *J. Biol. Chem.* **288**, 26121–26134 (2013).

33. Zhang, Y., Ma, Y., Gu, M. & Peng, Y. lncRNA TUG1 promotes the brown remodeling of white adipose tissue by regulating miR□204□targeted SIRT1 in diabetic mice. *Int. J. Mol. Med.* **46**, 2225–2234 (2020).

34. Hacisuleyman, E. *et al.* Topological organization of multichromosomal regions by the long intergenic noncoding RNA Firre. *Nat. Struct. Mol. Biol.* **21**, 198–206 (2014).

35. Lewandowski, J. P. *et al.* The Firre locus produces a trans-acting RNA molecule that functions in hematopoiesis. *Nat. Commun.* **10**, 5137 (2019).

36. Ishiura, H. *et al.* Noncoding CGG repeat expansions in neuronal intranuclear inclusion disease, oculopharyngodistal myopathy and an overlapping disease. *Nat. Genet.* **51**, 1222–1232 (2019).

37. He, Q. *et al.* Long noncoding RNA TUG1 facilitates osteogenic differentiation of periodontal ligament stem cells via interacting with Lin28A. *Cell Death Dis.* **9**, 455 (2018).

38. Yu, Y. *et al.* LncRNA TUG1 promoted osteogenic differentiation through promoting bFGF ubiquitination. *In Vitro Cell. Dev. Biol. Anim.* **56**, 42–48 (2020).

39. Wang, Y., Shi, Z. Y., Feng, J. & Cao, J. K. HDAC6 regulates dental mesenchymal stem cells and osteoclast differentiation. *BMC Oral Health* **18**, 190 (2018).

40. Sun, J. *et al.* HDAC6 Is Involved in the Histone Deacetylation of In Vitro Maturation Oocytes and the Reprogramming of Nuclear Transplantation in Pig. *Reprod. Sci. Thousand Oaks Calif* **28**, 2630–2640 (2021).

41. Hubbard, J. J. *et al.* Efficient iPS cell generation from blood using episomes and HDAC inhibitors. *J. Vis. Exp. JoVE* e52009 (2014) doi:10.3791/52009.

42. Cabili, M. N. *et al.* Localization and abundance analysis of human lncRNAs at single-cell and single-molecule resolution. *Genome Biol.* **16**, 20 (2015).

43. Chen, L.-L. Linking Long Noncoding RNA Localization and Function. *Trends Biochem. Sci.* **41**, 761–772 (2016).

44. Cho, S. W. *et al.* Promoter of lncRNA Gene PVT1 Is a Tumor-Suppressor DNA Boundary Element. *Cell* **173**, 1398-1412.e22 (2018).

45. Stojic, L. *et al.* Specificity of RNAi, LNA and CRISPRi as loss-of-function methods in transcriptional analysis. *Nucleic Acids Res.* **46**, 5950–5966 (2018).

46. Lennox, K. A. & Behlke, M. A. Cellular localization of long non-coding RNAs affects silencing by RNAi more than by antisense oligonucleotides. *Nucleic Acids Res.* **44**, 863–877 (2016).

47. Li, Y. *et al.* LINC00240 promotes gastric cancer cell proliferation, migration and EMT via the miR-124-3p / DNMT3B axis. *Cell Biochem. Funct.* **38**, 1079–1088 (2020).

48. Lewandowski, J. P. *et al.* The Tug1 lncRNA locus is essential for male fertility. *Genome Biol.* **21**, 237 (2020).

49. Lorenz, R. *et al.* ViennaRNA Package 2.0. *Algorithms Mol. Biol.* **6**, 26 (2011).

50. Pedersen, L., Hagedorn, P. H., Lindholm, M. W. & Lindow, M. A Kinetic Model Explains Why Shorter and Less Affine Enzyme-recruiting Oligonucleotides Can Be More Potent. *Mol. Ther. Nucleic Acids* **3**, e149 (2014).

51. Fusaki, N., Ban, H., Nishiyama, A., Saeki, K. & Hasegawa, M. Efficient induction of transgene-free human pluripotent stem cells using a vector based on Sendai virus, an RNA virus that does not integrate into the host genome. *Proc. Jpn. Acad. Ser. B Phys. Biol. Sci.* **85**, 348–362 (2009).

52. Schneider, C. A., Rasband, W. S. & Eliceiri, K. W. NIH Image to ImageJ: 25 years of image analysis. *Nat. Methods* **9**, 671–675 (2012).

53. Dobin, A. *et al.* STAR: ultrafast universal RNA-seq aligner. *Bioinforma. Oxf. Engl.* **29**, 15–21 (2013).

54. Andersson, R. *et al.* An atlas of active enhancers across human cell types and tissues. *Nature* **507**, 455–461 (2014).

55. Suzuki, H. *et al.* The transcriptional network that controls growth arrest and differentiation in a human myeloid leukemia cell line. *Nat. Genet.* **41**, 553–562 (2009).

56. Alam, T. *et al.* Comparative transcriptomics of primary cells in vertebrates. *Genome Res.* **30**, 951–961 (2020).

57. Arnold, P., Erb, I., Pachkov, M., Molina, N. & van Nimwegen, E. MotEvo: integrated Bayesian probabilistic methods for inferring regulatory sites and motifs on multiple alignments of DNA sequences. *Bioinforma. Oxf. Engl.* **28**, 487–494 (2012).

58. Pachkov, M., Balwierz, P. J., Arnold, P., Ozonov, E. & van Nimwegen, E. SwissRegulon, a database of genome-wide annotations of regulatory sites: recent updates. *Nucleic Acids Res.* **41**, D214-220 (2013).

59. Robinson, M. D., McCarthy, D. J. & Smyth, G. K. edgeR: a Bioconductor package for differential expression analysis of digital gene expression data. *Bioinformatics* **26**, 139–140 (2010).

60. Korotkevich, G. *et al.* Fast gene set enrichment analysis. *bioRvix* (2016) doi:10.1101/060012.

61. Kim, D. *et al.* TopHat2: accurate alignment of transcriptomes in the presence of insertions, deletions and gene fusions. *Genome Biol.* **14**, R36 (2013).

62. Love, M. I., Huber, W. & Anders, S. Moderated estimation of fold change and dispersion for RNA-seq data with DESeq2. *Genome Biol.* **15**, 550 (2014).

63. Kuo, C.-C. *et al.* Detection of RNA-DNA binding sites in long noncoding RNAs. *Nucleic Acids Res*. **47**, e32 (2019).

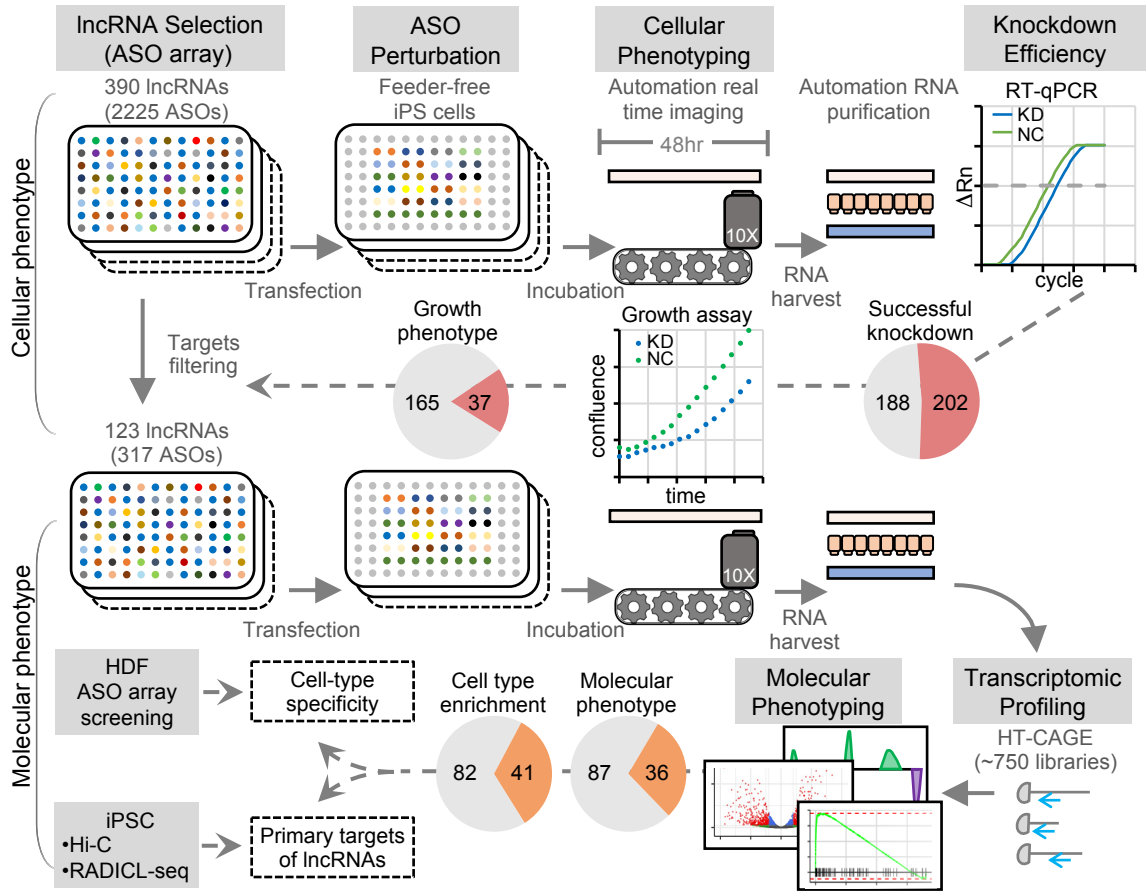

Fig. 1 Schematic of the ASO array screen for growth phenotype and molecular phenotype of lncRNAs.

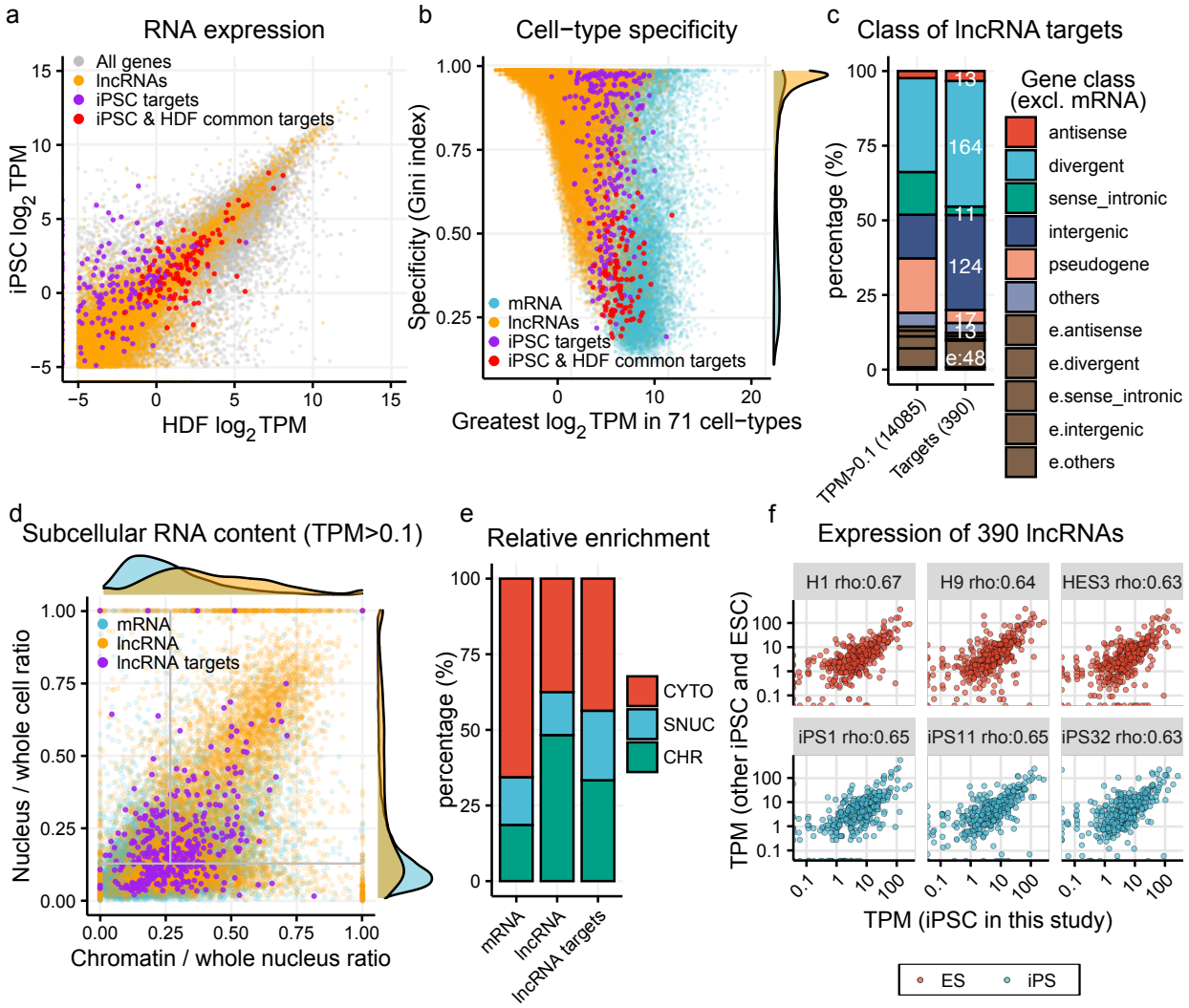

Figure S1. Properties of the 390 lncRNA targets. a, Gene expression level of iPSC and HDF derived from bulk RNA-sequencing on the native cells, highlighting the lncRNAs (orange), the screening targets in iPSC alone (purple) and the targets have been screened in both iPSC and HDF (red). **b**, Cell-type specificity according to the expression of each gene in 71 cell-types including iPS and ES. Gini index was calculated by comparing CAGE expression profiles of these cell-types. **c**, Gene class of the 390 lncRNA targets and their corresponding proportion in iPSC when applying different cutoffs of expression level determined by bulk RNA-sequencing. Coding mRNA was excluded from the proportion. **d**, Subcellular localization of expressed genes (TPM > 0.1, determined by bulk-RNA seq) in iPSC, showing coding mRNA (blue), lncRNA (yellow) and the 387 targets (purple, 3 targets were undetermined). Subcellular fractionation of iPSC was performed and followed by RNA-sequencing on the cytoplasmic, soluble nucleoplasmic and chromatin fractions. The nuclear ratio from the whole cell (y-axis) was calculated from the normalized TPMs for (SNUC + CHR)/(CYTO + SNUC + CHR). The chromatin ratio from the whole nucleus (x-axis) was calculated from the normalized TPMs for CHR / (SNUC + CHR). The regions represent enrichment to CHR (upper-right), SNUC (upper-left) and CYTO (bottom) are segmented by the grey lines, which are the median value of all the genes (>1 TPM) of the 2 axes. **e**, The relative enrichment of mRNAs, lncRNAs and the lncRNA targets in the 3 subcellular compartments, defined by the criteria described in (**d**). **f,** Expression level of the 390 lncRNAs in our iPS line and comparison to 3 other human iPS lines and 3 human ES lines from the FANTOM5 data.

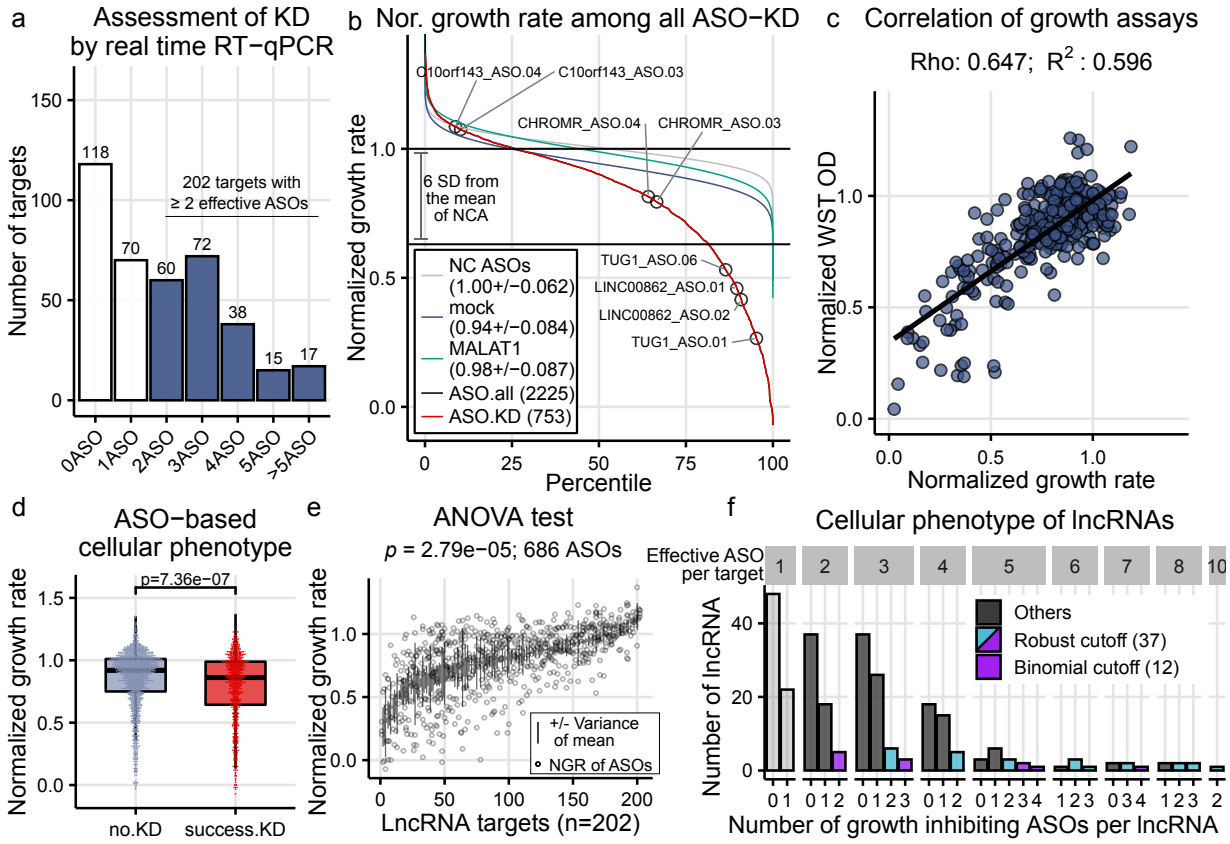

g

Correlation of knockdown and growth phenotype with gene properties

Target properties	Test	P-Value: KD (yes vs no)	P-Value: Growth inhibition (yes vs no)
TIR conservation	Wilcoxon (greater)	6.775.E-01	1.796.E-01
Exon conservation	Wilcoxon (greater)	3.176.E-01	8.709.E-01
Subcellular localization:			
Nucleus ratio in whole cell	Wilcoxon (greater)	**1.794.E-02***	5.725.E-01
Chromatin ratio in whole nucleus	Wilcoxon (greater)	3.748.E-01	4.652.E-01
Expression level			
CAGE log_2TPM	Wilcoxon (greater)	**1.950.E-03****	**2.124.E-02***
RNA-seq log_2TPM	Wilcoxon (greater)	**1.542.E-05****	8.994.E-02
Number of exons	Wilcoxon (greater)	**5.107.E-04****	4.679.E-01
Exosome sensitivity	Wilcoxon (less)	**3.764.E-04****	1.755.E-01
Cell-type specificity (Gini index)	Wilcoxon (less)	**2.578.E-03****	**7.848.E-05****
Cell-type specificity (% no express)	Wilcoxon (less)	**2.512.E-03****	**4.979.E-05****
# Hi-C interacting coding genes (10k)	Wilcoxon (greater)	7.952.E-01	6.402.E-02
# eQTL-linked coding genes	Wilcoxon (greater)	2.615.E-01	1.622.E-01
# RADICL-seq interacting coding genes	Wilcoxon (greater)	**8.360.E-05****	4.339.E-01

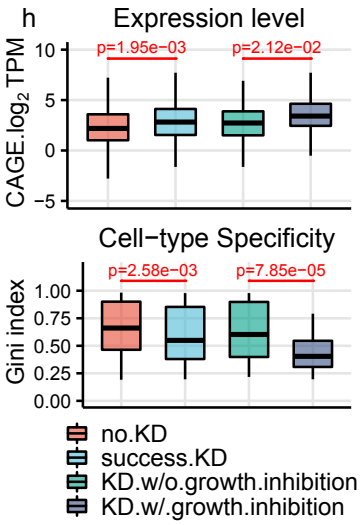

Fig. 2 Cellular phenotypes and their correlations with genomic properties of lncRNAs. a, Number of target with successful KD and the number of ASO showed KD from the targets. **b,** The distributions of normalized growth rate for all ASO KD. A cutoff of 0.63, which is 6 SD from the mean of the negative controls (cell transfected with NC ASO), was used to determine change of growth. **c,** Correlation between WST-1 growth assay and Incucyte growth assay in the ASO subset selected for CAGE profiling. **d,** Normalized growth rate of ASO with or without showing successful knockdown. **e**, Normalized growth rate of each ASO targeting the same lncRNAs and the variances of each lncRNA (686 ASOs for 202 lncRNAs). One-way ANOVA test resulted in a *p*-value as 2.79E-5. **f,** LncRNAs are defined as growth phenotype by at least 2 effective ASOs showing growth inhibition (robust cutoff, n= 37) and by the number of ASO passing binomial statistics (stringent cutoff, n=12). **g**, Table showing the *p*-value of the correlation tests between the genomic properties and the result of KD and growth phenotype (lncRNA targets, n=390; no.KD, n=188; KD, n=202; KD.growth, n=37; KD.no.growth, n=165; * <0.05, ** <0.01). **h**, Wilcoxon tests on expression level and cell-type specificity.

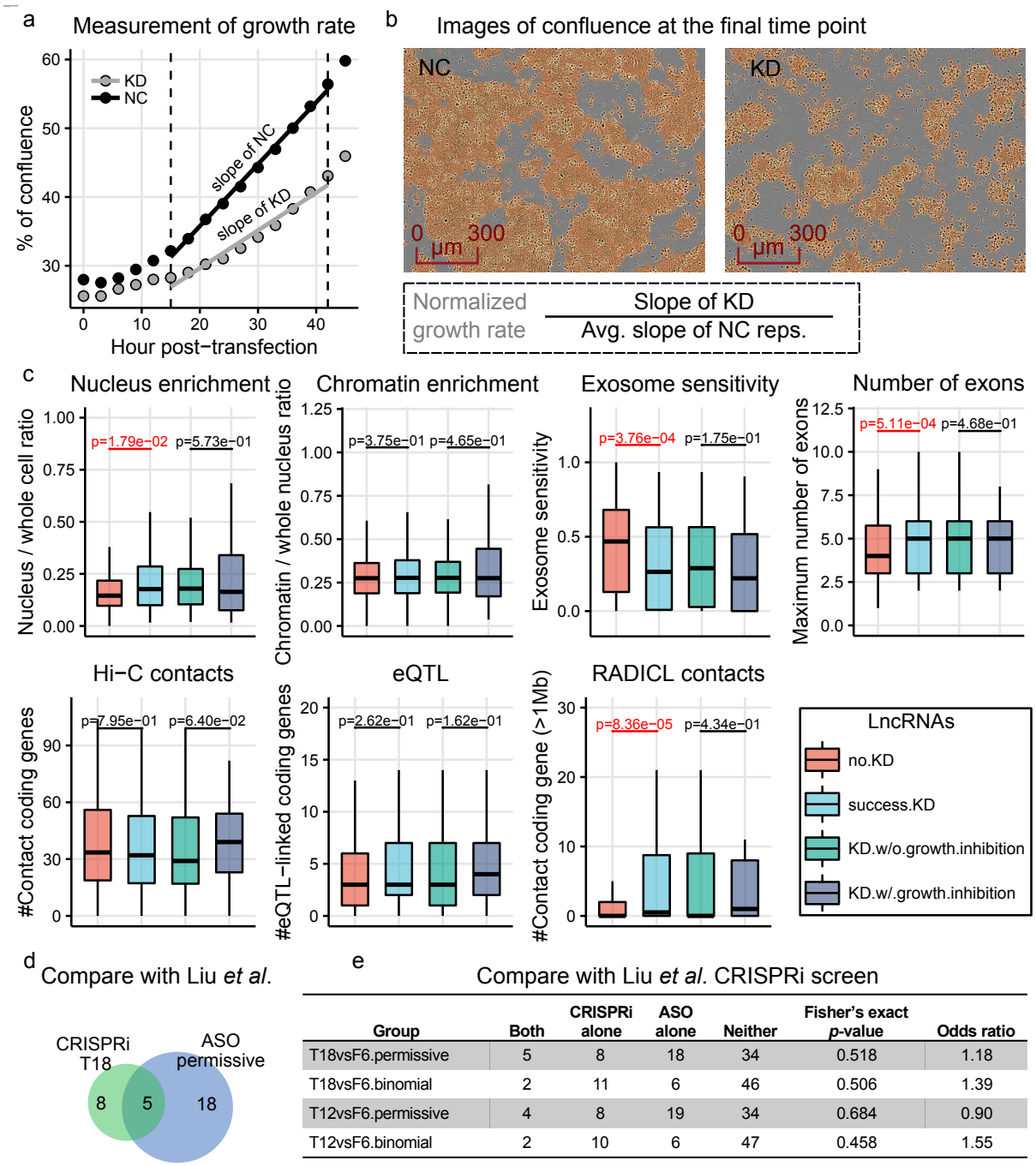

Group	Both	CRISPRi alone	ASO alone	Neither	Fisher's exact *p*-value	Odds ratio
T18vsF6.permissive	5	8	18	34	0.518	1.18
T18vsF6.binomial	2	11	6	46	0.506	1.39
T12vsF6.permissive	4	8	19	34	0.684	0.90
T12vsF6.binomial	2	10	6	47	0.458	1.55

Fig. S2 Cellular phenotypes and their correlations with genomic properties of lncRNAs. a, Growth rate of each KD sample was normalized by NC ASOs from the same set of experiment. **b,** Example images of NC and KD taken at the final time point are shown. **c,** LncRNAs with successful KD are more enriched in the nucleus**,** less exosome sensitive and have a greater number of exons. LIncRNAs with a growth phenotype show greater number of exons and greater number of Hi-C contacts (lncRNA targets, n=390; noKD, n=188; KD, n=202; KD.growth, n=37; KD.no.growth, n=165). *p*-value < 0.05, highlighted in red. **d**, Venn diagram showing the growth related lncRNAs from the 65 common lncRNAs targeted in the CRISPRi screen by Liu *et al*. and from this study. **e**, Fisher's exact tests compare the growth phenotype between the Liu *et al*. CRISPRi screen (2 time points) and this study (2 cutoffs).

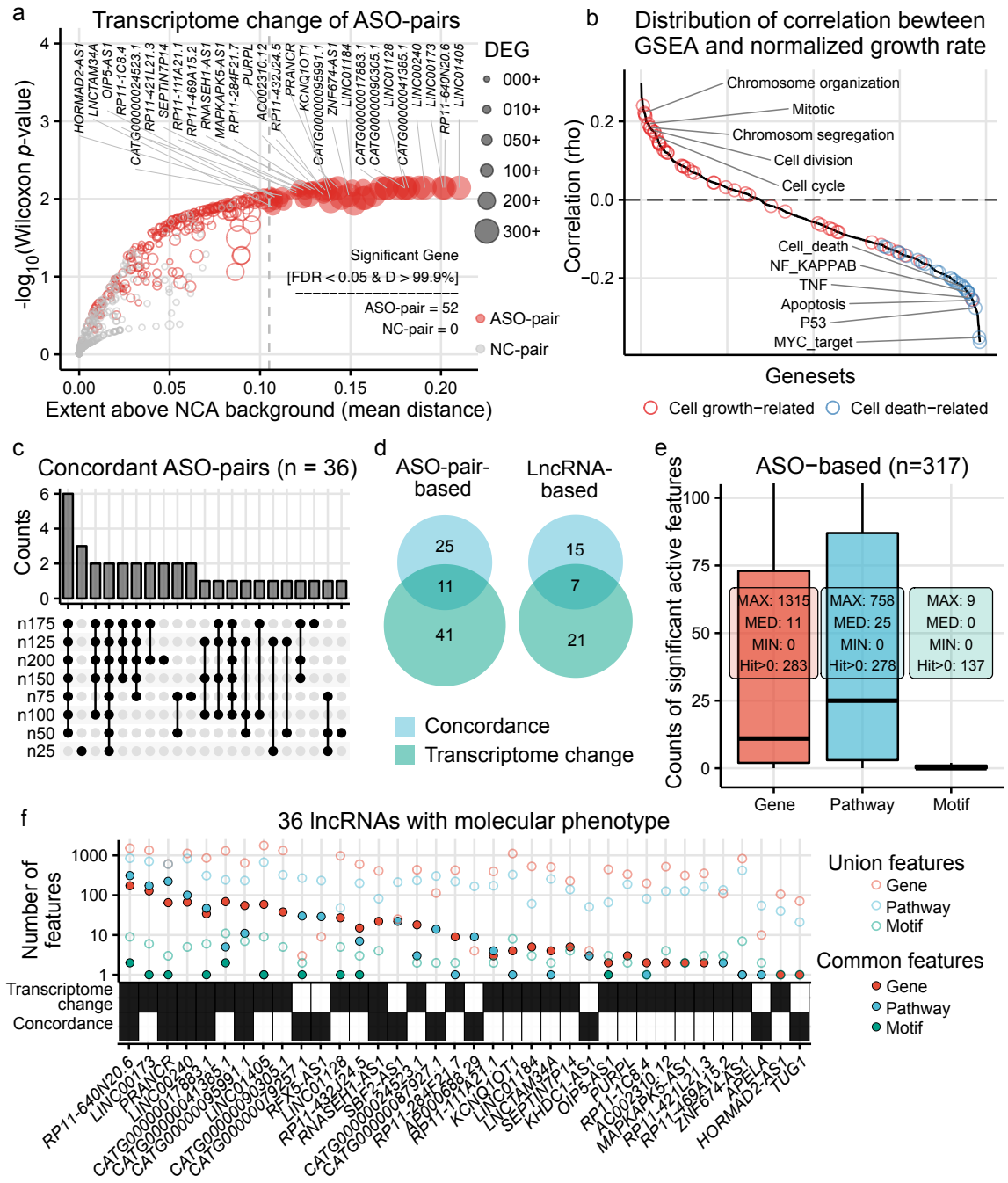

Fig.3 Molecular phenotypes of 123 lncRNAs. a, Visualization of the transcriptome changes of ASO-pairs after edgeR analysis. 52 ASO-pairs were considered to have significant transcriptomic change. **b**, Correlation between GSEA result for each pathway with the normalized growth rate across all the ASOs. **c**, Concordant ASO-pairs derived from different geneset sizes. **d**, ASO-pair-based and lncRNA-based Venn diagram showing the overlap of pairs/lncRNAs that are concordant and with reproducible transcriptome change. **e**, ASO-based results of number of significant differentially active molecular features in both up- and down-regulations (gene: *edgeR* FDR < 0.1, |across sample Z-Score| > 1.645; pathway: *fgsea* padj < 0.05, |across sample Z-Score| > 1.645; motif: MARA FDR < 0.1. **f**, Number of union significant features and common significant features of representative ASO-pairs of 36 lncRNAs showing molecular phenotype. The target lncRNAs are excluded from the number of differentially active genes. The representative ASO-pairs and the contents of significant features are shown in **Table S3**.

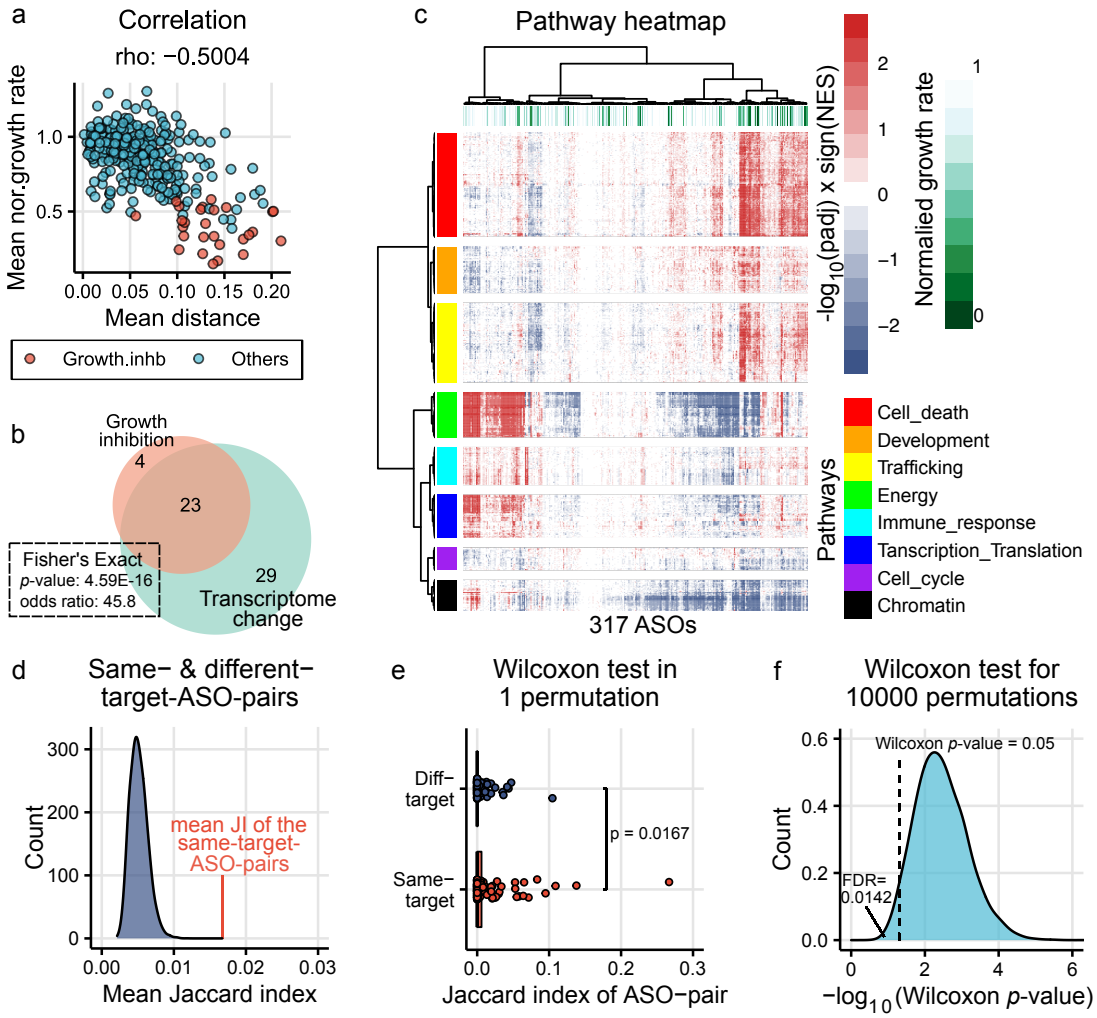

Fig.S3 Correlation between molecular phenotype and cellular phenotype and lncRNA target specific results. a, Correlation between global change and normalized growth rate for the 293 ASO-pairs. **b**, Venn diagram showing the significant ASO-pair hits of transcriptome change and growth inhibition. **c**, Heatmap from pathway *fgsea* analysis showing 317 ASOs. **d**, The distribution of mean Jaccard indices from the different-target-ASO-pair background and the mean Jaccard index of the same-target-ASO-pairs. Using the *edgeR* dataset using the cutoff of FDR < 0.1 & |across sample Z-Score| > 1.645, DEGs passing the cutoff from each ASO-knockdown were taken for 293 ASO- pairs while the same ASOs were permuted 10,000 times enforcing different-target pairing. The mean Jaccard indices were calculated for the same-target group and for each permutation of the different-target group. The empirical p-value (<0.0001) represents the chance that the mean of the Jaccard index of the same target group is not greater than the different-target group. **e**, Using the Jaccard index of overlap DEGs, non-redundant ASO-pairs (n=137) were selected randomly and the selected ASOs were permuted into different target pair for Wilcoxon test. The chart shows the result of one of the permutations. **f**, The p-value was recorded in each permutation and illustrated as $-\log_{10}$ *p*-value. False discovery rate of 0.0142 was calculated as 142/10,000 times where Wilcoxon *p*-value ≥ 0.05.

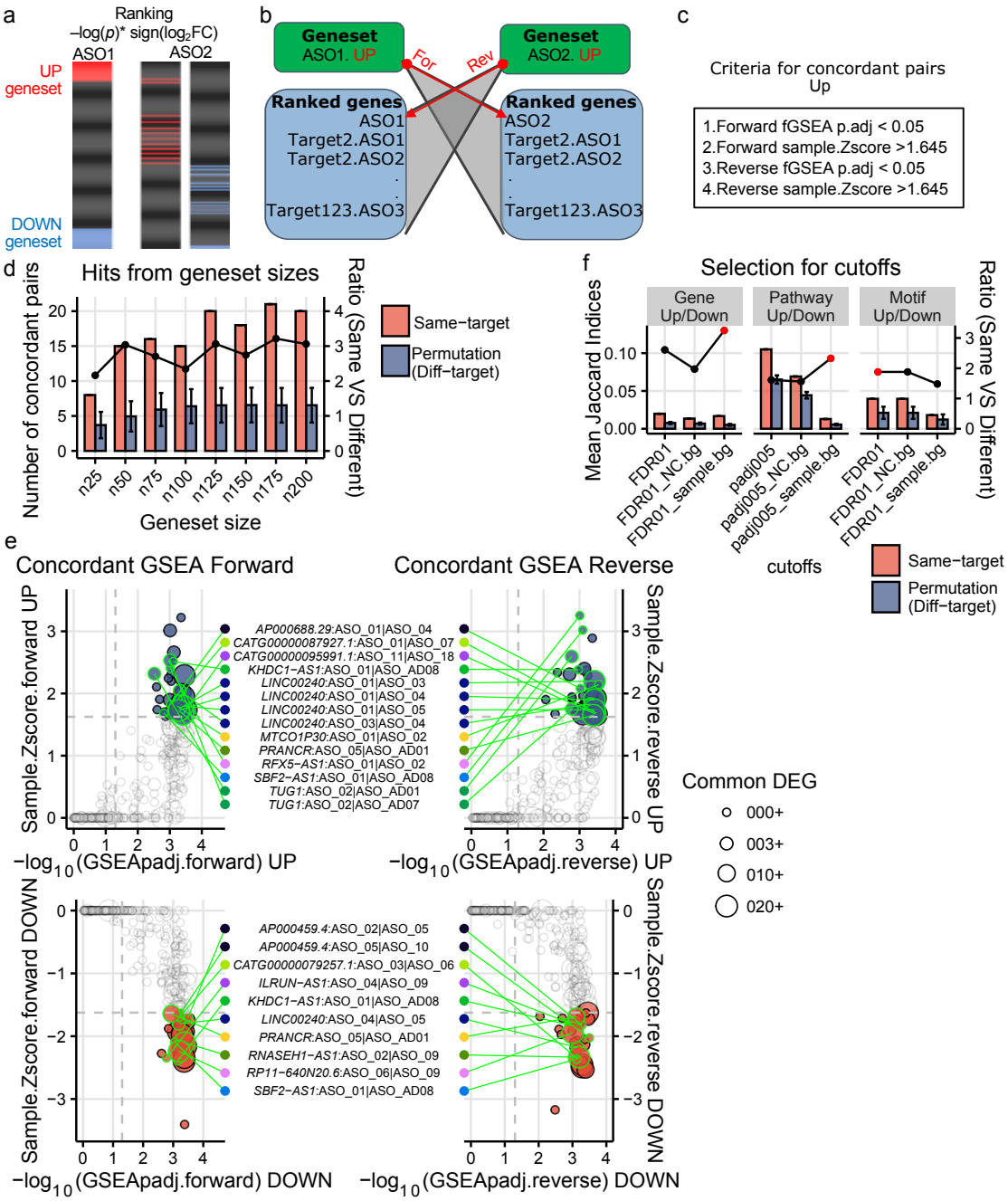

Fig. S4 Knockdown by ASO targeting the same lncRNA show concordant knockdown profiles. **a**, Diagram showing the method of reciprocal enrichment test, by selecting top and bottom ranked genes from the KD profile and testing for enrichment in another KD profile. **b**, Enrichment tests include forward and reverse analyses and each geneset was tested against all KD profiles from other lncRNA targets to generate sample-based background. **c**, Criteria of calling a hit for concordant ASO-pair. **d**, The numbers of concordant ASO-pairs defined by the criteria shown in (**c**) where all the geneset sizes shown significantly higher number of hits than the different-target-ASO-pair background (empirical *p*-value < 0.05). **e**, An example of concordant pairs defined by n125. **f**, Selection of cutoffs for significant differentially active features by Jaccard index. Under different cutoffs, the Jaccard indices reflecting the degree of overlap in ASO-pairs were taken for the same-target-ASO-pairs (n=293) and the different-target-ASO-pairs (10,000 permutation for 293 pairs). Same-target is significantly higher than

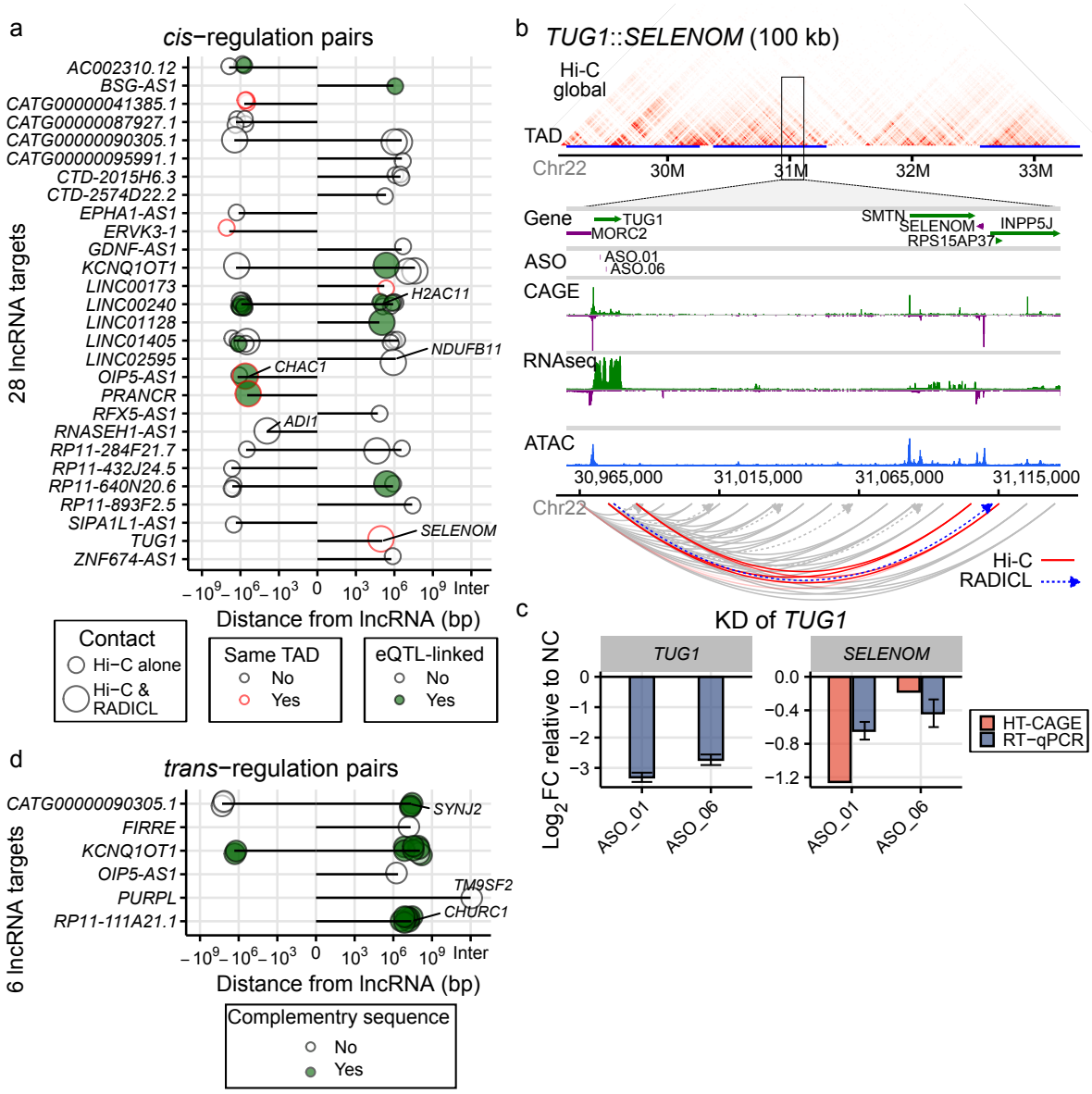

different-target in all tested cutoffs (empirical *p*-value < 0.05). Ratios (line plot) represent the mean of same-target-ASO-pairs divided by the mean of different-targets-ASO-pairs.

Fig. 4 Primary target of lncRNAs. a, A list of potential *cis*-regulation lncRNAs and their primary protein coding gene targets which are regulated significantly after knockdown (FDR < 0.1 & |Zscore| > 1.645). Hi-C contacts and TAD regions were defined at the resolutions of 10 kb and 50 kb, respectively. Within TAD: both contact regions located in the same TAD; eQTL-linked: linked-pairs with FDR < 0.25 from any of the 49 tissue samples. **b**, Genomic view of the *cis*-interaction between *TUG1* and *SELENOM*. **c**, Down-regulation of *SELENOM* upon ASO KD of *TUG1* from CAGE and an independent knockdown and RT-qPCR. **d**, 6 lncRNAs with potential *trans*-regulation for having RADICL-interacting protein coding genes (>1 Mb distance, no significant Hi-C contacts, detectable in HT-CAGE) with differential expression after knockdown (FDR < 0.1 & |Zscore| > 1.645). Complementary sequence similarity found from RNA transcripts towards the gene body of the protein coding genes.

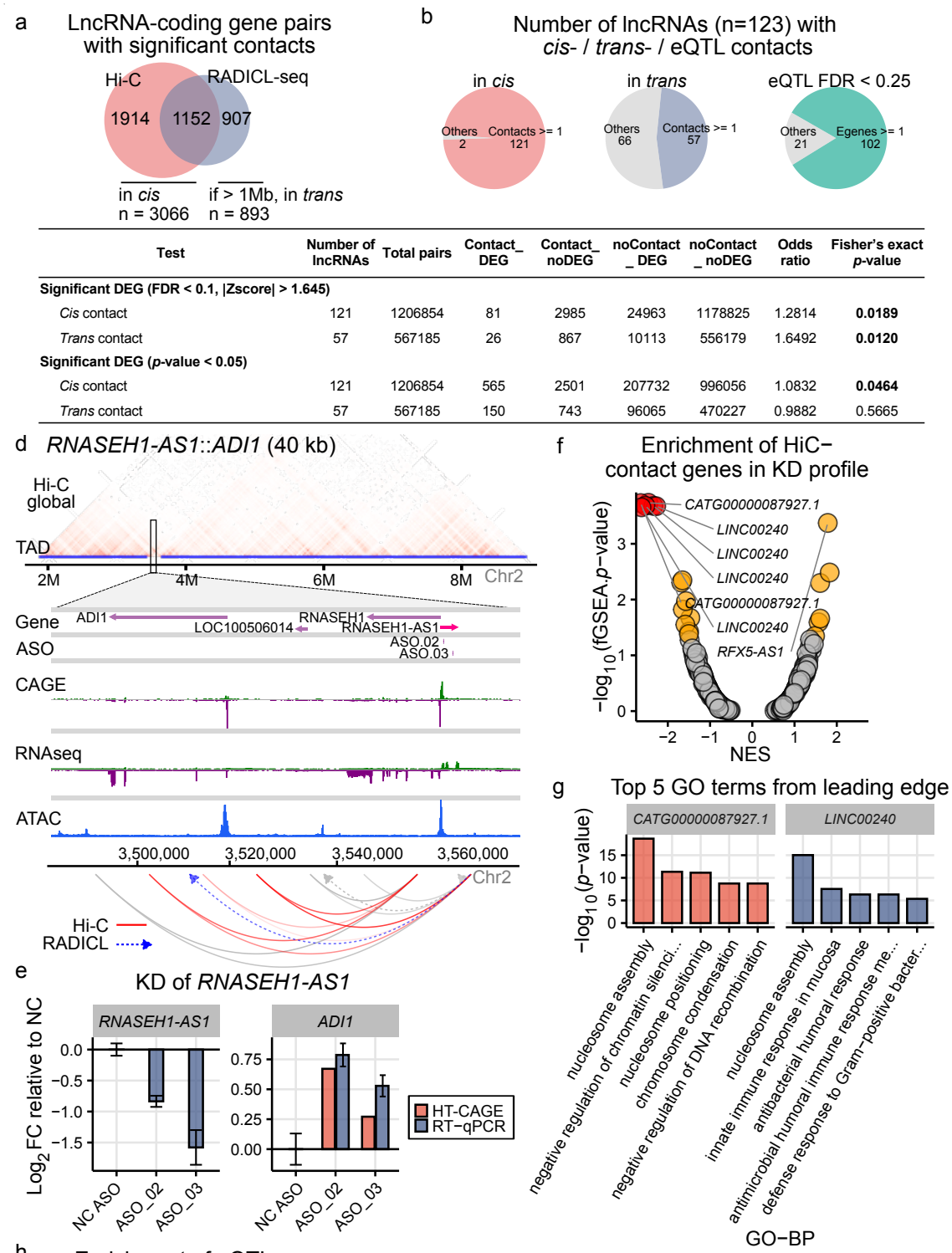

Test	Number of lncRNAs	Total pairs	Contact_ DEG	Contact_ noDEG	noContact _ DEG	noContact _ noDEG	Odds ratio	Fisher's exact *p*-value
Significant DEG (FDR < 0.1, |Zscore| > 1.645)								
Cis contact	121	1206854	81	2985	24963	1178825	1.2814	**0.0189**
Trans contact	57	567185	26	867	10113	556179	1.6492	**0.0120**
Significant DEG (*p*-value < 0.05)								
Cis contact	121	1206854	565	2501	207732	996056	1.0832	**0.0464**
Trans contact	57	567185	150	743	96065	470227	0.9882	0.5665

Fig.S5 Primary targets of lncRNAs identified by knockdown profiles and chromatin interaction. **a**, Number of lncRNA-protein coding gene pairs that showed significant interaction (FDR < 0.05) from Hi-C (10 kb resolution) and RADICL-seq (25 kb resolution) data of native iPS cells. Only protein coding genes detectable in HT-CAGE are included (n = 9974). Venn diagram showing the overlap of Hi-C and RADICL-seq identified pairs. Any pairs with Hi-C contacts are defined as *cis* interaction while pairs with only RADICL-seq contacts and with a minimum genomic distance great than 1 Mb are defined as *trans* interaction. **b**, Number of lncRNAs (n = 123) showing *cis* interaction, *trans* interaction or eQTL-linkage with other protein coding genes. **c**, Fisher's exact test for the enrichment of *cis*- and *trans*-contacts in significant differentially expressed genes upon knockdown. Only lncRNAs with at least one contact are included while all protein coding genes of selected lncRNAs are used in the analyses. **d**, Another example of Hi-C mediated regulation. Hi-C contacts and TAD regions were defined at the resolutions of 10 kb and 50 kb, respectively. **e**, *RNASEH1-AS1* KD led to up-regulation of *ADI1* from the HT-CAGE result and an independent KD followed by RT-qPCR. **f**, Enrichment of the Hi-C contact gene sets were tested against the KD profiles for each of the 121 lncRNAs (312 ASOs). Red, FDR < 0.05; yellow, *p*-value < 0.05. **g**, TopGo analysis on the leading edge genes for Hi-C contacts enrichment in KD profile showing the top 5 biological process GO terms. **h**, Enrichment of the eQTL linked gene sets were tested against the KD profiles for 102 lncRNAs (267 ASOs).

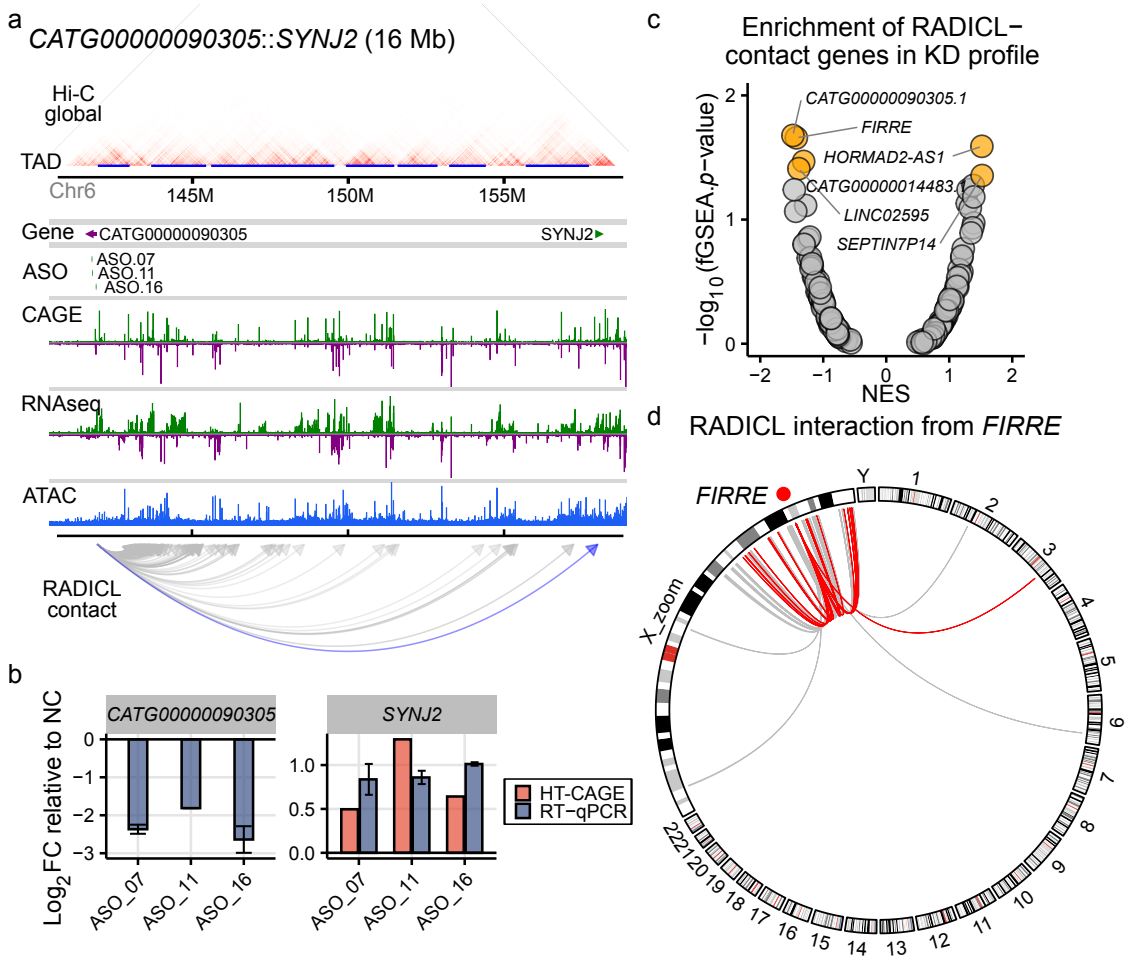

Fig.S6 Primary targets of lncRNAs identified by knockdown profiles and RADICL-seq. a, Genomic view of the RADICL-interaction between *CATG00000090305* and *SYNJ2*. **b**, Up-regulation of *SYNJ2* after the KD of *CATG0000090305* was shown in HT-CAGE and was validated by RT-qPCR. **c**, Enrichment analysis to determine if the RADICL-seq contact gene sets for each of the 64 lncRNAs (149 ASOs) enriched in the KD profiles. **d**, Circos plot illustrating RADICL interactions with *FIRRE* where only contacts with protein coding genes >1 Mb from the lncRNAs without significant Hi-C contacts were included. Grey lines: interactions from RADICL-seq, red lines: RADICL interactions and leading edge genes from the enrichment analysis in **c**.

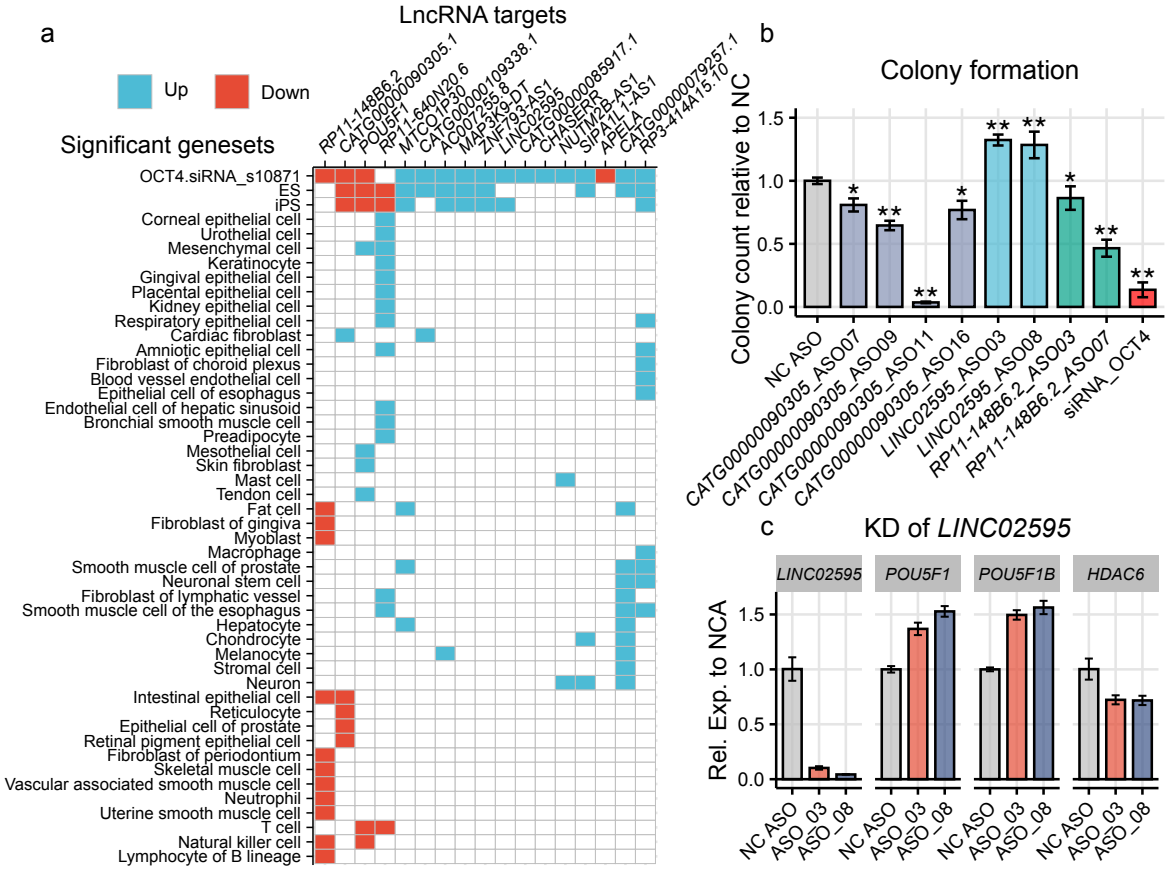

Fig.5 Enrichment of cell-type specific genes upon lncRNA perturbation. a, Expressed genes from a cell-type were ranked according to the specificity scores derived from Gini index of 71 cell-types. Expression level of a gene in a cell-type in the lower 5 percentile among the 71 cell-types is considered non-expressed. Eight genesets were generated from each cell-type by selecting the top 25, 50, 75, 100, 125, 150, 175 and 200 cell-type specific genes. Genesets were tested for enrichment in all the ASO-KD profiles to acquire p.adj of *fgsea* and across sample Z-score on NES. LncRNA targets having at least 2 ASOs with NES in the same direction, p.adj < 0.05 and |Z-score| > 1.645 are shown in the heatmap. Only lncRNAs enriched with stem-related gene sets are shown, full list is in **Fig. S7a**. **b**, Colony formation assay upon the knockdown of *CATG00000090305*, *LINC02595*, *RP11-148B6.2* and OCT4. The number of colonies were counted 6 days after the cells were seeded by crystal violet staining. The chart shows the mean and standard deviation of 3 independent assays. **c**, Knockdown of *LINC02595* with spontaneous differentiation condition, RNA levels relative to NC ASO-transfected samples of *LINC02595*, *POU5F1*, *POU5F1B* and *HDAC6* are shown.

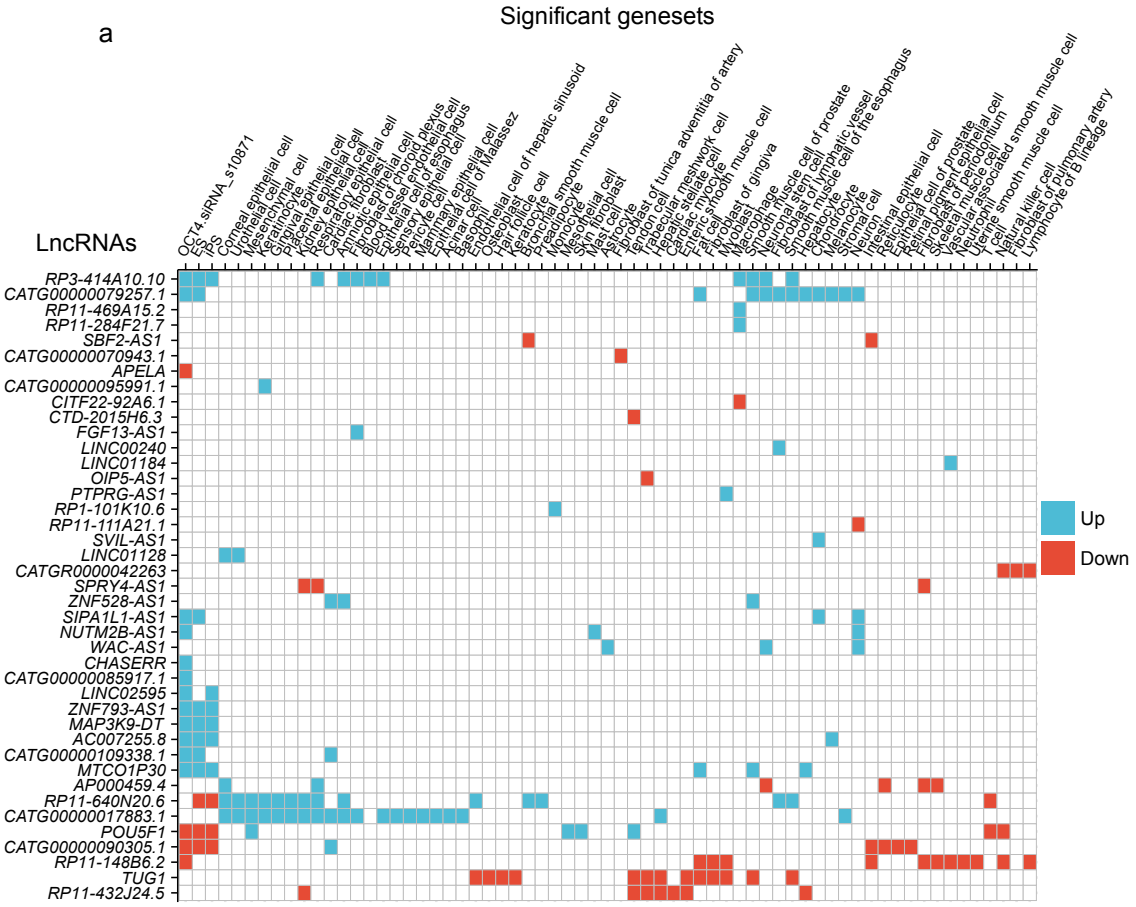

Fig.S7 Enrichment of cell-type specific genes upon lncRNA perturbation. a, Expressed genes from a cell-type were ranked according to the specificity scores derived from Gini index of 71 cell-types. Expression level of a gene in a cell-type in the lower 5th percentile among the 71 cell-types is considered non-expressed. Eight genesets were generated from each cell-type by selecting the top 25, 50, 75, 100, 125, 150, 175 and 200 cell-type specific genes. Genesets were tested for enrichment in all the ASO-KD profiles to acquire p.adj of fgsea and across sample Z-score on NES. LncRNA targets having at least 2 ASOs with NES in the same direction, p.adj < 0.05 and |Z-score| > 1.645 are shown in the heatmap.

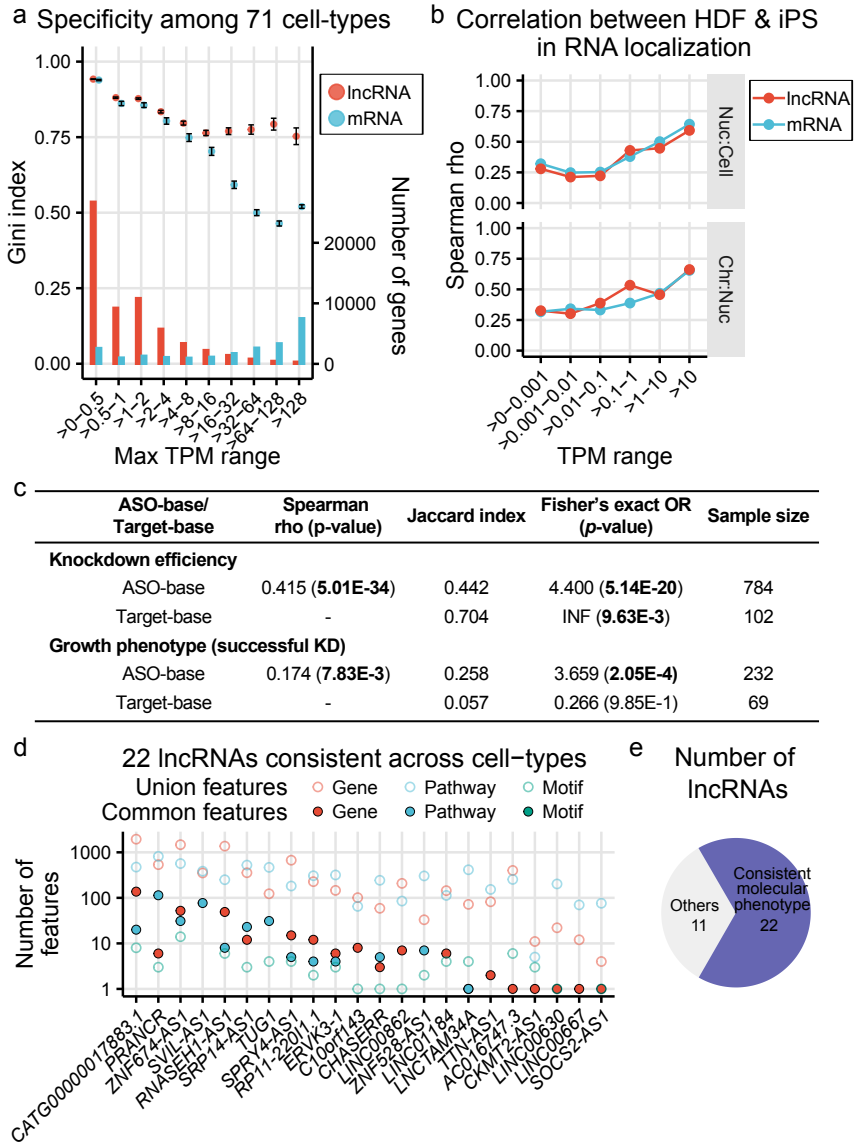

ASO-base/ Target-base	Spearman rho (p-value)	Jaccard index	Fisher's exact OR (*p*-value)	Sample size
Knockdown efficiency				
ASO-base	0.415 (**5.01E-34**)	0.442	4.400 (**5.14E-20**)	784
Target-base	-	0.704	INF (**9.63E-3**)	102
Growth phenotype (successful KD)				
ASO-base	0.174 (**7.83E-3**)	0.258	3.659 (**2.05E-4**)	232
Target-base	-	0.057	0.266 (9.85E-1)	69

Fig. 6 Comparison of lncRNAs between HDF and iPS cells. a, Cell-type specificity at expression level. Gini index was calculated by comparing CAGE expression profiles of 71 cell-types including iPS and ES cells. The mean Gini index and 95% confidence interval was shown for mRNA and lncRNA at each expression level bin, which was determined by the greatest TPM of each gene among the 71 cell-types. **b**, Spearman correlation of the nucleus-to-whole cell ratio and the chromatin-to-whole nucleus ratio between HDF and iPS cells. The correlation was divided into mRNA and lncRNA in different expression level bins. **c**, The comparison of KD efficiency and growth phenotype of the same sets of lncRNA targets between HDF and iPS cells. For Jaccard index and Fisher's exact, the cutoff of KD is 50% while the cut off of growth phenotype is normalized growth rate < 0.63. OR: odds ratio. **d**, Number of union significant features and common significant features of representative ASO-pairs of 22 lncRNAs showing consistent molecular phenotype across HDF and iPS cells. The target lncRNAs are excluded from the number of differentially active genes. The representative ASO-pairs and the contents of significant features are shown in **Table S6**. **e**, Pie chart summarizing the number of lncRNAs with consistent molecular phenotype across HDF and iPS cells.

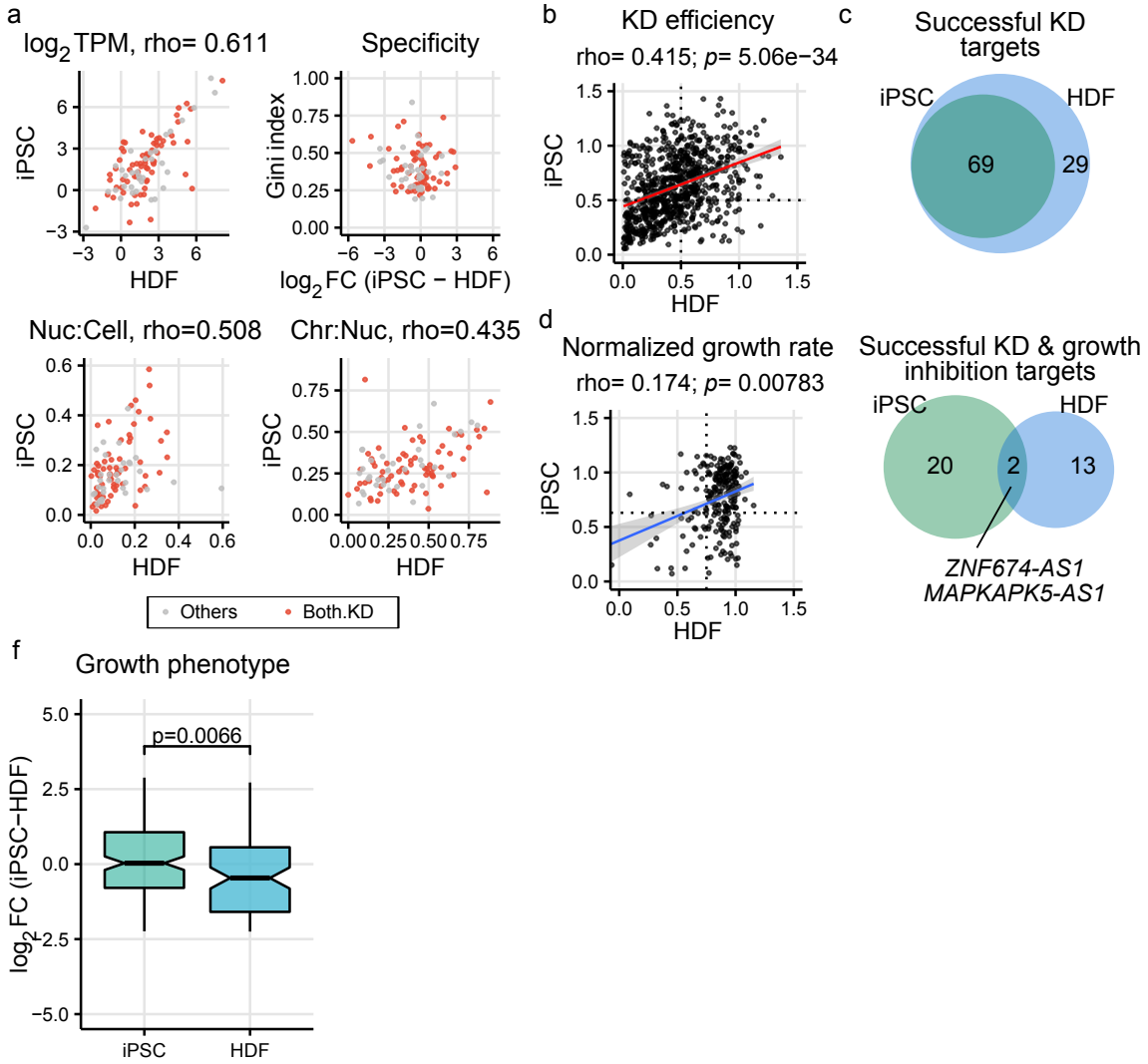

Fig.S8 Cell-type specificity of lncRNAs between HDF and iPS cells. a, Comparison on the expression level, subcellular localization ratio and cell-type specificity between HDF and iPS cells of the 102 assayed lncRNAs. **b**, Correlation of KD efficiency at ASO-level. **c**, Venn diagram showing the overlap successful KD at target-level. **d**, Correlation of normalized growth rate of all the effective ASOs. **e**, Venn diagram showing the overlap lncRNAs with growth phenotype at target-level. **f**, Log_2FC of transcriptomes between HDF and iPS cells was obtained from CAGE followed by edgeR analysis. Log_2FC of 20 lncRNA targets showing growth phenotypes in iPS cells and 13 targets showing growth phenotype in HDF were compared by Wilcoxon test.

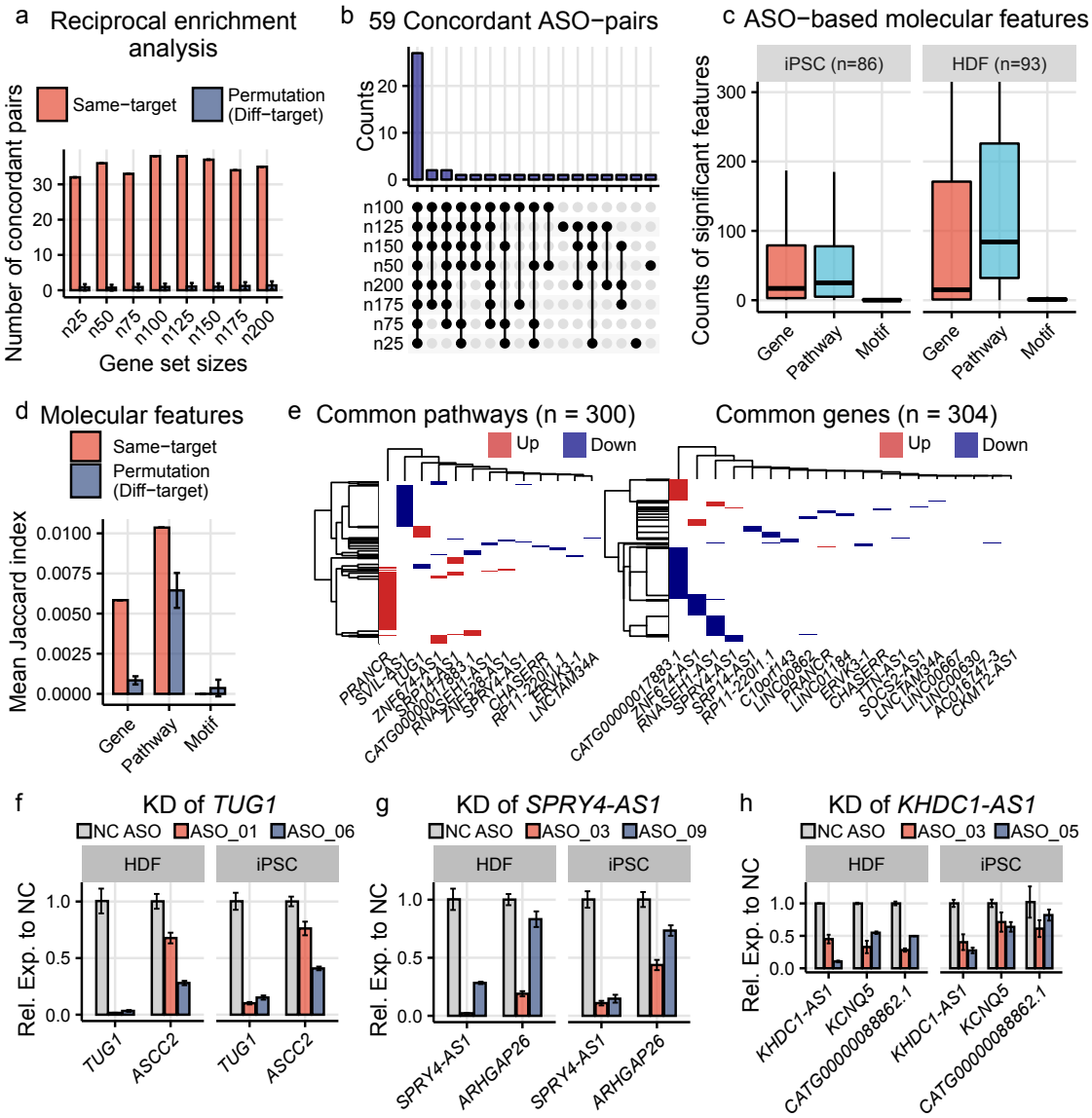

Fig.S9 Consistent molecular phenotype of lncRNAs in HDF and iPS cells. a, Number of concordant ASO-pairs from the same-target and from the different-target permutation in all the tested geneset sizes. **b**, Plot showing the number of concordant ASO-pairs from different geneset sizes. **c**, Boxplot showing the number of significant differential active molecular features (ASOs from the 33 common lncRNAs) where the lncRNA target is excluded from the count of genes. Significant criteria: iPS-gene, FDR < 0.1, abs(across-sample Z-score) > 1.645; iPS-pathway, FDR<0.05, , abs(across-sample Z-score) > 1.645; iPS-motif, FDR<0.1, abs(across-sample Z-score) > 1.645; HDF-gene, FDR < 0.01, abs(across-sample Z-score) > 1.645, abs($\log_2$FC) > 0.5; HDF-pathway, FDR<0.05, abs(across-sample Z-score) > 1.645, abs(NES) > 1; HDF-motif, FDR<0.05, abs(across-sample Z-score) > 1.645. **d**, Using overlap significant differential active features to determine concordance of the same-target-ASO-pairs and compare to different-target pairs with 10,000 permutations. Significant criteria were described in **c**. **e**, Heatmaps showing commonly up- and down-regulated pathways and genes in both HDF and iPSC upon knockdown. The representative ASO-pair used for each lncRNA was shown in **table S6**. **e&f,** Knockdown of TUG1 and SPRY4-AS1 shows regulation on their *cis*-regulated genes in both HDF and iPS cells. **g**, Knockdown of *KHDC1-AS1* resulted in similarly *cis*-regulation on *KCNQ5* and *CATG00000088862.1* in both HDF and iPS cells.

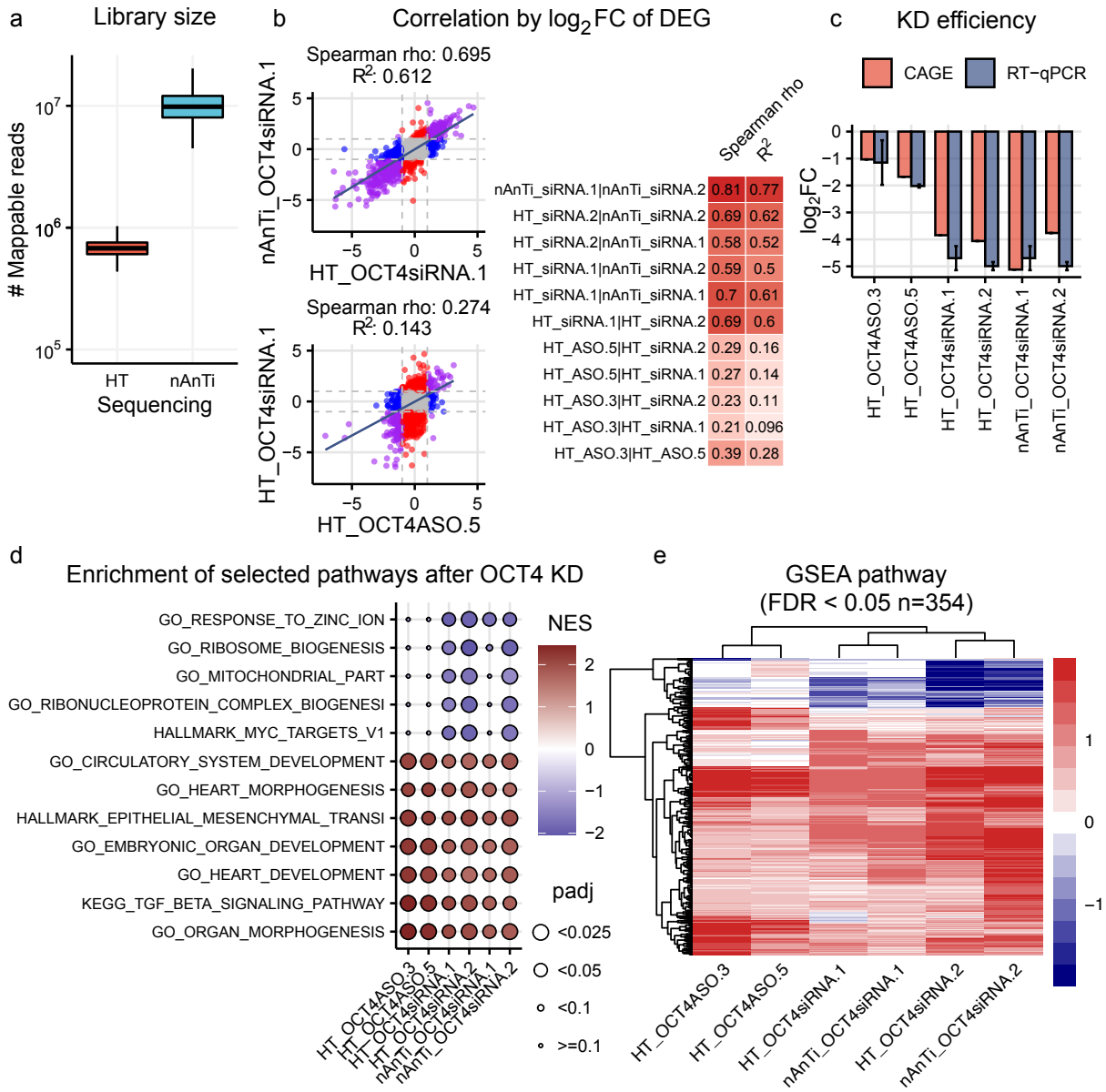

Fig. S10 Comparison between nAnTi-CAGE and HT-CAGE; and comparison between ASO response and siRNA response using OCT4 KD in iPS cells. a, The mappable library sizes of HT-CAGE of this study and the mean mappable library size of nAnTi-CAGE in the HDF KD study. **b**, Correlation of different KD profiles using the $\log_2$FC determined by edgeR analyses. **c**, The KD efficiency of OCT4 ASO and siRNA determined by CAGE and RT-qPCR. **d**, 12 selected pathways upon KD of OCT4 ranked by the absolute NES of the 6 KD profiles from GSEA analyses. **e**, Heatmap of all the significant GSEA pathways showing -log10(FDR) * sign(NES) of the 6 KD profiles.